INVESTIGATION OF TEXTURE DEVELOPMENT AND PORTEVIN-LE CHATELIER BANDS IN 5754 ALUMINUM ALLOY

A THESIS SUBMITTED TO
THE GRADUATE SCHOOL OF NATURAL AND APPLIED SCIENCES
OF
MIDDLE EAST TECHNICAL UNIVERSITY

BY

ORHAN BERK AYTUNA

IN PARTIAL FULFILLMENT OF THE REQUIREMENTS
FOR
THE DEGREE OF MASTER OF SCIENCE
IN
METALLURGICAL AND MATERIALS ENGINEERING

NOVEMBER 2019

Approval of the thesis:

INVESTIGATION OF TEXTURE DEVELOPMENT AND PORTEVIN-LE CHATELIER BANDS IN 5754 ALUMINUM ALLOY

submitted by **ORHAN BERK AYTUNA** in partial fulfillment of the requirements for the degree of **Master of Science in Metallurgical and Materials Engineering Department, Middle East Technical University** by,

Prof. Dr. Halil Kalıpçılar
Dean, Graduate School of **Natural and Applied Sciences** ________________

Prof. Dr. Cemil Hakan Gür
Head of Department, **Met. and Mat. Eng.** ________________

Assoc. Prof. Dr. Mert Efe
Supervisor, **Met. and Mat. Eng., METU** ________________

Examining Committee Members:

Prof. Dr. Cemil Hakan Gür
Met. and Mat. Eng., METU ________________

Assoc. Prof. Dr. Mert Efe
Met. and Mat. Eng., METU ________________

Prof. Dr. Bilgehan Ögel
Met. and Mat. Eng., METU ________________

Assoc. Prof. Dr. Caner Şimşir
Met. and Mat. Eng., METU ________________

Assist. Prof. Dr. Eda Aydoğan Güngör
Integrated Manufacturing Research and Application Center,
Sabancı University ________________

Date: 22.11.2019

I hereby declare that all information in this document has been obtained and presented in accordance with academic rules and ethical conduct. I also declare that, as required by these rules and conduct, I have fully cited and referenced all material and results that are not original to this work.

Name, Surname: Orhan Berk Aytuna

Signature:

ABSTRACT

INVESTIGATION OF TEXTURE DEVELOPMENT AND PORTEVIN-LE CHATELIER BANDS IN 5754 ALUMINUM ALLOY

Aytuna, Orhan Berk
Master of Science, Metallurgical and Materials Engineering
Supervisor: Assoc. Prof. Dr. Mert Efe

November 2019, 78 pages

Texture and microstructure are substantial parameters for final products which are made of non-heat treatable aluminum alloys such as 5xxx series. Optimizing these parameters is possible via deformation processes and following heat treatments. In this thesis; hot and cold rolling operation, as a basic deformation process, was applied to the aluminum and resulting copper, brass and cube type of texture was investigated. Effects of different annealing parameters on the deformed specimens were also analyzed with texture development and microstructural features such as recrystallization and abnormal grain growth. It was also detected that mechanical behavior of this alloy was also affected by nucleation and propagation of Portevin-Le Chatelier bands under various strain paths. Therefore, an in-plane biaxial test apparatus was utilized with a miniature cruciform specimen to achieve uniaxial and equibiaxial strain paths. The magnitude of load serrations and inhomogeneous strain distributions due to PLC effect were examined with load cells and digital image correlation technique, respectively. Under biaxial stretching, PLC bands nucleated and propagated repeatedly at the same region of the specimen, while their formation was random under uniaxial tension. Due to shear stresses in uniaxial tension, PLC bands were promoted and evolved into sharp visible shear bands which cause eventual failure of product. Texture analysis also confirmed the emergence of shear components and cube texture with increasing strain. Conversely, biaxial deformation conditions were beneficial for prevention of undesired fracture from shear bands even if PLC strain contribution to the total strain was higher than uniaxial conditions.

Keywords: PLC, DIC, Biaxial, Forming, Texture

ÖZ

5754 ALÜMİNYUM ALAŞIMINDA DOKU GELİŞİMİNİN VE PORTEVIN-LE CHATELIER BANTLARININ İNCELENMESİ

Aytuna, Orhan Berk
Yüksek Lisans, Metalurji ve Malzeme Mühendisliği
Tez Danışmanı: Doç. Dr. Mert Efe

Kasım 2019, 78 sayfa

Doku ve mikro yapı, 5xxx serisi gibi ısıl işlem uygulanamayan alüminyum alaşımlarından yapılan son ürün için önemli parametrelerdir. Bu parametreleri optimize etmek, deformasyon süreçleriyle ve bunları takip eden ısıl işlemlerle mümkündür. Bu tez çalışmasında; alüminyuma temel deformasyon işlemlerinden birisi olan sıcak ve soğuk haddeleme işlemi uygulanmış ve bunun sonucunda oluşan bakır, pirinç ve küp tipi dokular incelenmiştir. Farklı tavlama parametrelerinin deforme olmuş numuneler üzerindeki etkileri de doku gelişimiyle ve mikro yapısal özelliklerle (yeniden kristallenme ve anormal tane büyümesi gibi) analiz edilmiştir. Bunlara ek olarak, bu alaşımın mekanik davranışının PLC bantlarının çeşitli gerinim izleri altında çekirdeklenmesinden ve çoğalmasından da etkilendiği tespit edilmiştir. Bu doğrultuda, tek eksenli ve çift eksenli gerilme yollarını elde etmek amacıyla minyatür bir artı şeklinde numune ile çift eksenli test cihazı kullanılmıştır. PLC etkisinden dolayı yük dalgalanmalarının büyüklüğü ve homojen olmayan gerinim dağılımları sırasıyla yük hücreleri ve dijital görüntü korelasyonu tekniği ile incelenmiştir. Çift eksenli gerilim altında, PLC bantları numunenin aynı bölgesinde birbirini tekrar edecek şekilde çekirdeklenip ilerlerken, bantların oluşumu tek eksenli gerilim altında rastgele olmuştur. Tek eksenli koşuldaki kesme kuvvetleri nedeniyle, PLC bantları artmış ve ürünün sonunda kırılmasına neden olan keskin ve görünür kesme bantlarına dönüşmüştür. Ayrıca doku analizi, kesme bileşenlerinin ve küp dokusunun artan gerilme ile ortaya çıktığını doğrulamıştır. Diğer taraftan; çift eksenli çekme koşulunda PLC bantlarının gerinimlerinin toplam gerinime katkısı daha fazla gözlemlense de kesme bantlarından istenmeyen kırılma bu koşullar altında baskılanmıştır ve engellenmiştir.

Anahtar Kelimeler: PLC, DIC, Çift-eksenli, Şekillendirme, Doku

To my beloved family

ACKNOWLEDGEMENTS

This work was supported by European Commission's Research Executive Agency's Marie Skłodowska-Curie Actions – Career Integration Grant (FP7-PEOPLE-2013-CIG) with grant agreement #631774.

Firstly, I would like to thank my advisor Dr. Mert EFE for his suggestions and encouragement. I feel very lucky to be guided by him since I knocked his door. I learned to make research on many fields instead of just focusing on my thesis topic. I am grateful to him for being my mentor in my first academic experience. For future, I wish him all the best in the U.S.

I would like to thank my all labmates for sharing information about anything and helping me in experiments; Kıvanç ALKAN, Berkay BAYRAMİN, Yılmaz AKIN, Merve ÇOBANOĞLU, Mustafa BALCILAR and especially Baran GÜLER who is the man of discipline and efficiency. I am also grateful to Dr. Osman El-Atwani to visit our lab and take part in our experiments. I feel lucky to work on joint project with him.

I am thankful to all staff of service laboratories in Metallurgical and Materials Engineering. I am grateful to Dr. Süha TİRKEŞ and Welding Technologies and NDT Center to allow me to prepare my specimens in their workshop.

I especially thank to İbrahim AYDIN and Anıl ERDAL for their sincere friendship during my graduate life. I am also grateful to Burak ALDOĞAN, Esra SÜTÇÜ, Seren ÖZER, Eda AYSAL, Pelin GÜNDOĞMUŞ and Bersu AZER.

Many thanks to Elif YEŞİLAY with all my heart for the most meaningful support. For today and future, I cannot imagine any success or decision without her.

Lastly, I would like to dedicate this work to my family, Sevda and Mustafa Önder AYTUNA. They have been my lovely supporters all my life who never expect anything in return. Many thanks for continuous support, help and patience.

TABLE OF CONTENTS

CHAPTERS

LIST OF TABLES

TABLES

LIST OF FIGURES

FIGURES

CHAPTER 1

INTRODUCTION

5754 aluminum alloys whose major alloying element is Magnesium (up to 6% in weight) are the non-heat treatable (strain hardenable) type of aluminum alloys. Their superior properties are good forming behavior, weldability and corrosion resistance characteristics [1]. Especially, if there is a need for higher strength from these alloys, they are mostly preferred in the form of wrought condition with O (annealed) or H (strain hardened) tempers [2]. For this purpose, understanding the deformation characteristics of this class of aluminum alloy has great importance.

To optimize the performance of these alloys for different applications, deformation behavior study should include microstructure and texture evolution with applied deformation and following annealing treatments. The texture of the aluminum alloys is mostly studied in the literature with rolling processes and typical rolling texture is known as the copper type texture. Secondly, in FCC metals, brass type of texture is another crucial texture mostly seen in these materials. These types of textures are generally the result of cold deformation [3]. Another important texture for aluminum is the cube texture. Excessive strain at high temperatures (hot rolling) or shear-based deformation leads to the formation of cube components in the texture [4].

In this thesis, texture change of the material after cold and hot rolling was investigated with Electron Backscatter Diffraction (EBSD). The reason of choosing rolling as a deformation process is its simplicity and common usage in the industry. compared to other processes. The material initially having copper texture was deformed with milling machine. For cold rolling, chosen reduction in thickness values were 33% and 66%. For hot rolling, the deformation temperature and reduction in thickness values were 480°C and 33%, respectively. All specimens after deformation were annealed at

345°C for 1.5 hours. Also, annealing was done at higher temperature (510°C) with shorter time intervals for investigating abnormal grain growth of cold rolled specimens. Resulting texture types (e.g. copper, brass and cube) and microstructures of deformed and annealed specimens were investigated and discussed.

Although texture is a very critical parameter for the strength, formability and other isotropic properties of the alloys and it is also studied in this work, the main factor affecting the deformation behavior of Al-Mg alloys is perceived as Portevin-Le Chatelier bands. Before optimizing the texture for different strain paths such as uniaxial, equibiaxial, etc. understanding the behavior of these bands has a significant role under different deformation states.

PLC bands are unique plastic instabilities observed mostly in alloys having solute atoms. Al-Mg alloys are common examples showing deformation behavior based on the PLC bands. Presence of solute Mg atoms and their interaction (breakaway and pinning) with the mobile (gliding) dislocations or other obstacles causes dynamic strain aging in micro-scale [5-9]. At macro scale, the PLC bands appear as angled and narrow strain localized lines during plastic deformation [10,11]. PLC bands cause heterogeneous deformation as a result of stress and strain jumps (serrations in flow curves) and the consequence is undesired visual sharp surface irregularities (shear bands) that can act as a stress concentrator for the catastrophic failures [12-14]. Since 5xxx Al alloys are used in the automotive industry due to their sufficient strength, good formability and good corrosion characteristics [15], irregularities that affect these properties i.e., poor surface finish after shaping operations should not be desirable. On the other hand, dynamic strain aging phenomena lead to negative strain rate sensitivity [16], which affects the mechanical response of Al-Mg alloys negatively during shaping and complicates the optimization of shaping parameters because of causing loss of ductility and undesired strain localization.

PLC band characteristics basically depend on two factors; strain rate [17] and temperature [18]. Variation of these two factors results in a different sequence of nucleation and propagation of PLC bands such as continuous (type A), discontinuous (type B) or random (type C) [19]. Factors apart from strain rate and temperature; grain size [14], precipitates [20], heat treatment [21], surface irregularities [13] or specimen shapes [22] also affects the PLC formation in Al-Mg alloys. Nonetheless, most of the previous studies used the uniaxial loading [17-24] to understand the deformation characteristics. Few studies in the literature focused on PLC bands under different strain paths. These studies include observation of PLC band formation region with hydraulic bulge testing [25], yield loci or yield surface of Al-Mg alloys [26,27], PLC band detection with thermal observation techniques instead of digital image correlation [28], forming and fracture strains of Al-Mg alloys [29] or hardening behavior and serration types under uniaxial, plain strain and biaxial condition [30]. However, a systematic study under various strain paths is needed for the detailed characterization of the shape and contribution of individual PLC bands and their effects on the fracture and deformation mode. It is well known that under uniaxial loading, fracture occurs from localized shear bands [10,13,31,32]. The shear stress state under uniaxial tension is responsible from this and it may also affect the PLC band formation. There is no macroscopic shear stress under biaxial tension, on the other hand, and the PLC formation may be different than the uniaxial.

Overall, after some trials of investigation of microstructure and texture with different rolling and annealing conditions, it was detected that PLC bands in the Al-Mg alloys have a more critical role in deformation characteristics. For this reason, the behavior of PLC bands in Al-Mg alloy was investigated under uniaxial and equibiaxial conditions in order to test the effect of strain path on their formation. An in-plane biaxial testing apparatus with strain analysis capability was utilized for this purpose. Firstly, the shape of the bands and strain amount in the bands were analyzed with the DIC technique. Digital image correlation technique as an optical method could analyze spatio-temporal characteristics of these bands by displaying strain field of the focused region (commonly gage length). When the PLC band nucleates at any area in that region, the strain distribution map has angled strain localized band(s) (generally

50°-60° to the tensile axis) [33,34]. This certain bands could provide information about nucleation or propagation characteristics of PLC bands depending on adjusted fps of CCD cameras. In other words, the type of propagation (A, B or C) could be described. After observing connections of PLC bands and the deformation mode characteristics of the material under different loading conditions, PLC band contribution to the failure was established. Finally, texture evolution during deformation was investigated under the different strain paths and PLC conditions to investigate their combined effects on the final texture, which is a critical feature controlling the overall formability of Al sheets.

CHAPTER 2

LITERATURE REVIEW

2.1. 5xxx Series of Aluminum Alloys

2.1.1. Background

Aluminum and its alloys are most widely used non-ferrous metals in the world. Their inimitable properties (corrosion resistance, lightweight, strength and low cost) make the aluminum mostly preferred in the industries. Although the need for the aluminum and its alloys still increases as technology evolving, common industries widely using aluminum are as follows:

- Production of automobiles and trucks,
- Packaging of food and beverages,
- Construction of buildings,
- Transmission of electricity,
- Development of transportation infrastructures,
- Production of defense and aerospace equipment,
- Manufacture of machinery and tools
- Production of durable consumer products [35].

Achieving the desired properties of aluminum needs some alloying elements in the composition. Together with alloying elements, there are many known types of alloy systems based on aluminum. Some of them are aluminum-copper, aluminum-lithium, aluminum-magnesium, aluminum-manganese, aluminum-silicon, aluminum-zinc, etc. Not only a combination of two elements exists, but also three elements systems were discovered, such as aluminum-copper-silicon, aluminum-copper-magnesium, aluminum-magnesium-zinc, etc. [37] Aluminum alloys having Magnesium element in the range of 0.5 to 6.0 % in weight (given in Figure 2.1) are called 5xxx series.

Magnesium is preferred because of its lightweight. These alloys have an ideal combination of strength and formability due to high strain hardening as result of dislocation structures after cold rolling and elements in the solid solution [36]. As an example; some mechanical, thermal and physical properties of 5754 aluminum alloys are given in Table 2.1. Effects of addition of magnesium element (especially for 5x54 alloys) are:

- Increasing ultimate tensile strength up to 15% Mg content by weight,
- Increasing tensile elongation after the initial decrease up to 10% Mg content by weight,
- Decreasing stacking fault energy, so decreasing cross-slip ability,
- Increasing work hardening rate,
- Increasing corrosion resistance (even in salt water) and
- Increasing weldability [37].

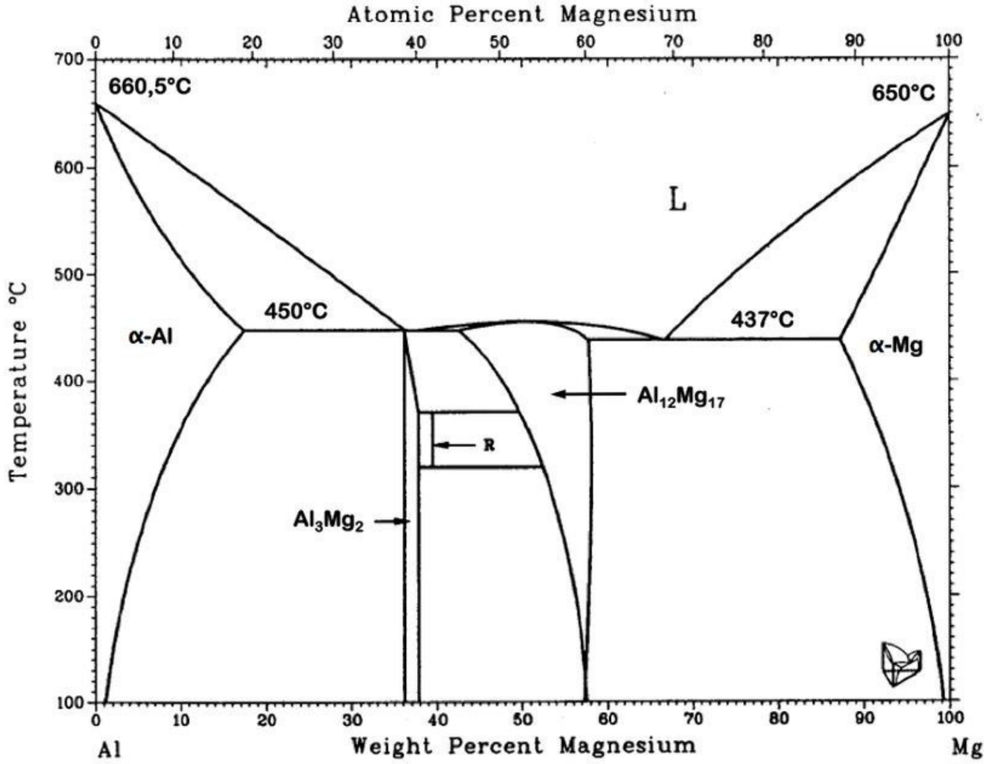

Figure 2.1. Aluminum-magnesium phase diagram [38]

Table 2.1. Some selected properties of 5754 aluminum alloy [39]

Property	Value	Property	Value
Density	2.66 g/cm^3	***Elastic Modulus***	68 GPa
Melting Point	600°C	***Yield Strength***	min. 130 MPa
Thermal Expansion	24x10^{-6}/K	***Tensile Strength***	220-270 MPa
Thermal Conductivity	147 W/m.K	***Hardness***	63 HB
Electrical Resistivity	0.049x10^{-6} Ω.m	***Elongation***	min. 7%

The classification of 5xxx aluminum alloys can be done as structural and automotive. For automotive alloys; strength, corrosion resistance and formability are main considerations. Especially, alloys having O-temper is suitable for the deep drawing applications and specifically, 5754 alloys are used when parts are exposed temperatures exceeding 100°C. On the other hand, strength after welding operation is the main criteria for structural aluminum alloys. Increase in Mg, Mn or Cr content maintain the strength of the material after welding operation [40].

2.1.2. Strengthening & deformation mechanism

The effect of magnesium atoms in the aluminum matrix is most importantly strengthening and increasing work hardening. Figure 2.2a illustrates effect of Mg addition on the mechanical properties of 5xxx alloys. Yield and tensile strength are affected positively by the presence of Mg atoms up to certain amount. Conversely, the elongation is dropped by approximately 30% at the beginning, but increases after 2% addition of Mg atoms in weight. During work hardening, increase in Mg contents causes rapid increase in lattice strain and increasing retained strain. Therefore, dislocation mobility decreases due to low stacking fault energy and dislocation amount increases. The overall result is high strength caused by solid solution strengthening by Mg atoms and strain-hardening by high dislocation amount and homogenous dislocation distribution as shown in Figure 2.2b [37].

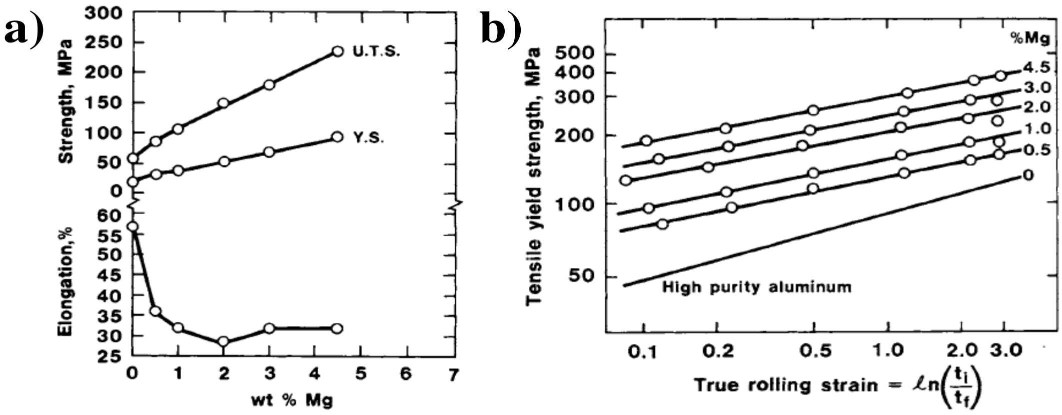

Figure 2.2. Improved mechanical properties of 5xxx Aluminum alloys by a) addition of Mg atoms b) combination of work hardening and addition of Mg atoms [37]

Aluminum alloys’ forming operation generally end up with localized strain and ductile fracture and it is affected by strain paths. Ductile fracture also occurs by void formation and localized strain in the shear bands. This deformation characteristic is optimized by the adding alloying elements to aluminum. Most widely preferred element is Magnesium for good formability. Some transition elements such as chromium and manganese are also added to modify microstructure of the material. However, for 5xxx series of aluminum alloys, magnesium alloys tend to diffuse through dislocations and restrict the work hardening behavior as a result of pinning action between dislocations and solute magnesium alloys [41]. The strength and formability of the Al-Mg alloys are based on the solid-solution hardening. It also improves the mechanical properties of aluminum alloy during sheet forming by suppressing local neck formation [15]. However, solid-solution strengthening becomes less effective at higher temperatures because of faster diffusion [35].

5xxx aluminum alloys as a non-heat treatable alloys are generally in the form of cold worked or hot worked. Generally, strain hardening rate is lower than the annealed condition for both cold and hot worked condition. Strain hardening behavior of these alloys is highly affected by the temperature of deformation. For 5456 aluminum alloys, increasing rolling temperatures decrease the tensile and yield strength and increase the elongation of the alloy. This softening is as a result of thermal recovery just after the deformation [1].

2.2. Texture of Aluminum

One of the parameters affecting the deformation characteristics of the metals or alloys is their textures. Texture can be mainly defined as differences in orientation of each neighbor grains in the polycrystalline structure [42]. Since metallic materials are crystalline, texture is very critical parameter for some mechanical, physical or optical properties. All shaping processes (forming, casting etc.), heat treatments (annealing, quenching etc.), joining processes (brazing, welding etc.) can change texture of metals.

The classification of texture can include casting texture, deformation texture and annealing texture. For FCC and BCC metals, grains tend to grow along [100] direction during casting. On the other hand, for HCP metals, deviation from ideal close packing (c/a=1.633) decides the formation of texture. For annealing textures, two important points are orientation of the nuclei and orientation dependence of grain growth phenomena. While recrystallization texture is controlled by these factors, there are no texture change during recovery stage. For both recovery and recrystallization texture, manufacturing history of metals plays important role. Since most of the metallic materials are produced with cold or hot shaping operations, deformation is pioneer factor for texture of metals. For deformation textures, crystal texture and extent of plastic deformation are main factors. In the presence of sufficient deformation, grains are oriented in preferred direction which depends on active deformation systems such as twinning or slip [43]. Deformation texture is studied most commonly with rolling process. For FCC and BCC structures typical fibre formations is given in Table 2.2 and orientation of these fibres is given in Figure 2.3 [44].

Table 2.2. Different texture components in metals and their Miller indices and Euler angles [44]

Fibre	Miller indices {hkl]<uvw> or Miller index description	Euler angles $\varphi_1, \varphi_2, \varphi_3$
α (FCC)	<110>//ND	
α (BCC)	<110>//RD	
γ	<111>//ND	
θ	<100>//ND	
τ	<110>//TD	
Copper	{112}<111>	90, 35, 45
S	{123}<634>	59, 37, 63
Goss	{011}<100>	0, 45, 90
Brass	{011}<211>	35, 45, 90
Dillamore	{4 4 11}<11 11 8>	90, 27, 45
Cube	{001}<100>	0, 0, 0

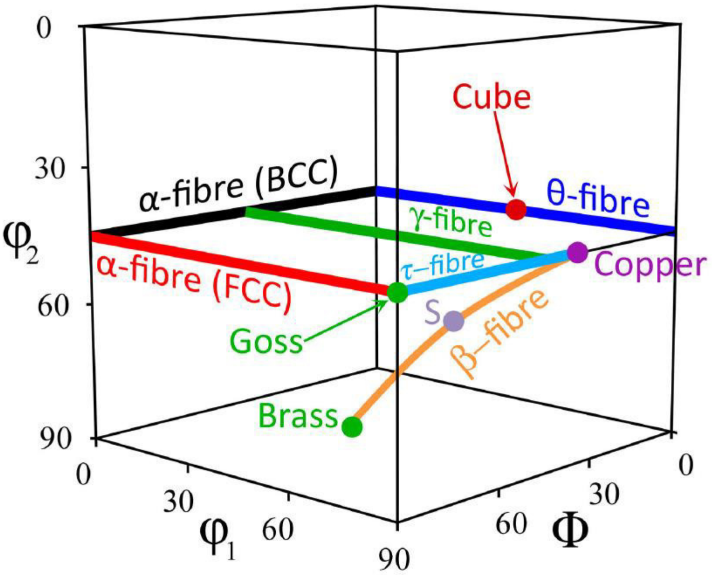

Figure 2.3. Different texture components for cubic metals [44]

Understating the deformation textures of FCC materials can help to understand texture of aluminum alloys. Stacking fault energy is the main criteria for formation of texture in FCC metals. The amount of stacking fault energy can be classified as high

(Aluminum ~170 mJm^{-2}), intermediate (Copper ~80 mJm^{-2}) and low (Alloys < 25 mJm^{-2}) [45,46]. In metals having low stacking fault energy, α-fibre is more significant than materials having high stacking fault energy [42]. Generally, aluminum alloys show strict texture types from beginning of the production steps to the end of that. These steps include casting, hot rolling, cold rolling and annealing like which of other metals. Figure 2.4 shows the microstructure and texture evolution of aluminum alloys according to mentioned production steps. The casting texture of aluminum alloys is random and grain size is large compared to microstructure after other deformation processes. Recrystallized grain structure of hot rolling results in typical cube texture. The cube texture changes to typical rolling texture of aluminum which is called copper texture [47]. For this study, there are three critical texture. These are;

- Cube texture
- Copper texture
- Brass texture

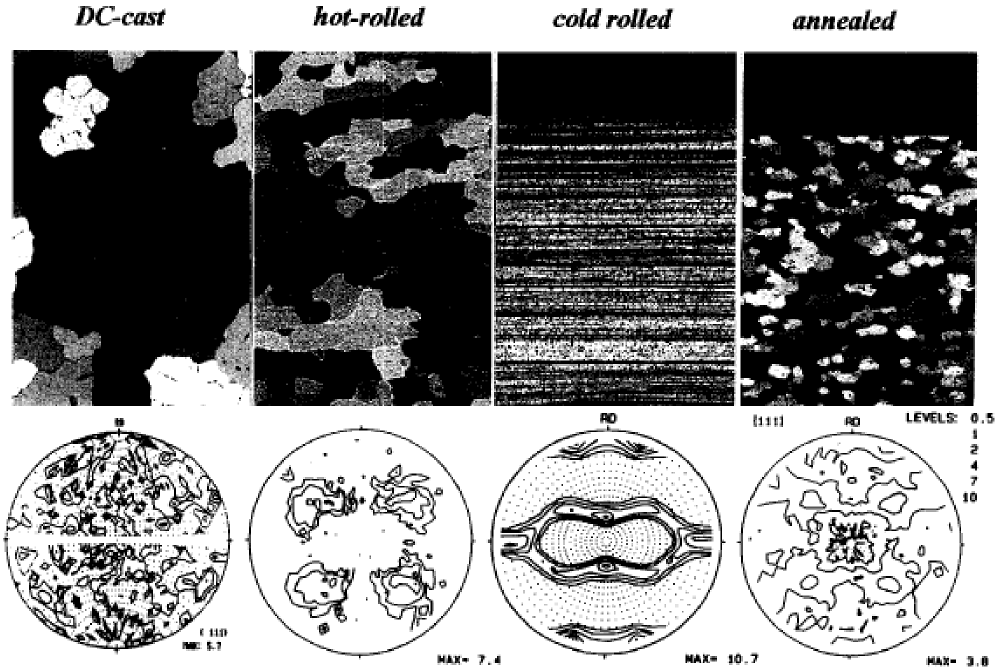

Figure 2.4. Microstructures and 111 pole figures of aluminum alloy for different processes [47]

2.2.1. Cube texture

Cube texture is dominant texture for pure aluminum after sufficient amount of cold deformation and annealing. For heat treatable and non-heat treatable aluminum alloys, cube component can be seen after hot rolling and fast cooling from high temperatures required for final solution annealing [15,48].

Cube component of the texture is also more stable component and deformation of the cube texture is more uniform during processes. As a result of these stability and deformation characteristics, nuclei having cube orientation can be formed quickly and growth and coalescence of subgrains from these nuclei takes place. Shear action of deformation processes can also create the nucleation sites for cube component during extra deformation [4]. Moreover, recrystallized cube grains have advantages over grains having other orientations and deformation of initial cube grains adds new sites of formation of cube nuclei for aluminum alloys [49].

2.2.2. Copper texture

Copper texture is also known as pure metal deformation texture in the literature and seen in the FCC metals like copper, aluminum etc. The other criteria of copper texture formation is high stacking fault energy [3]. The typical pole figure of copper texture is given in Figure 2.5a. Generally, copper texture has {123}<412> and {146}<112> orientations. In copper texture, the orientation of {112}<111> is obvious [43,44].

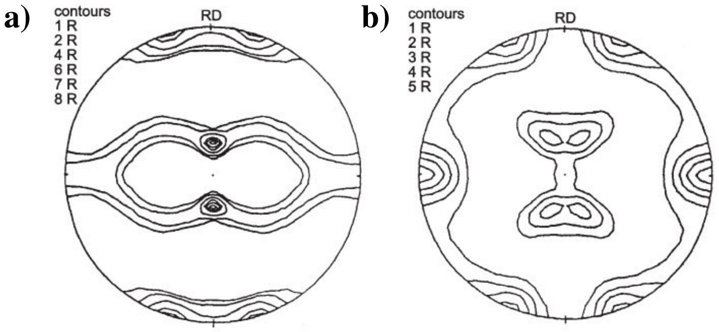

Figure 2.5. 111 pole figures for deformation texture of aluminum a) copper type b) brass type [3]

2.2.3. Brass texture

In brass texture, {110}<112> sharp orientations component is seen after rolling operations as show in Figure 2.5b. Instead of pure metals, alloys tend to form brass texture because of their low stacking fault energies [3]. Also, it is known that under biaxial condition, formation of brass texture is observed in the literature. Higher deformation amounts for equibiaxial conditions results in sharper brass component peaks in the pole figure. Figure 2.6 summarizes that under uniaxial conditions, formation of cube texture is desired whereas while the deformation path changes from uniaxial to equibiaxial, the texture becomes brass type [50,51].

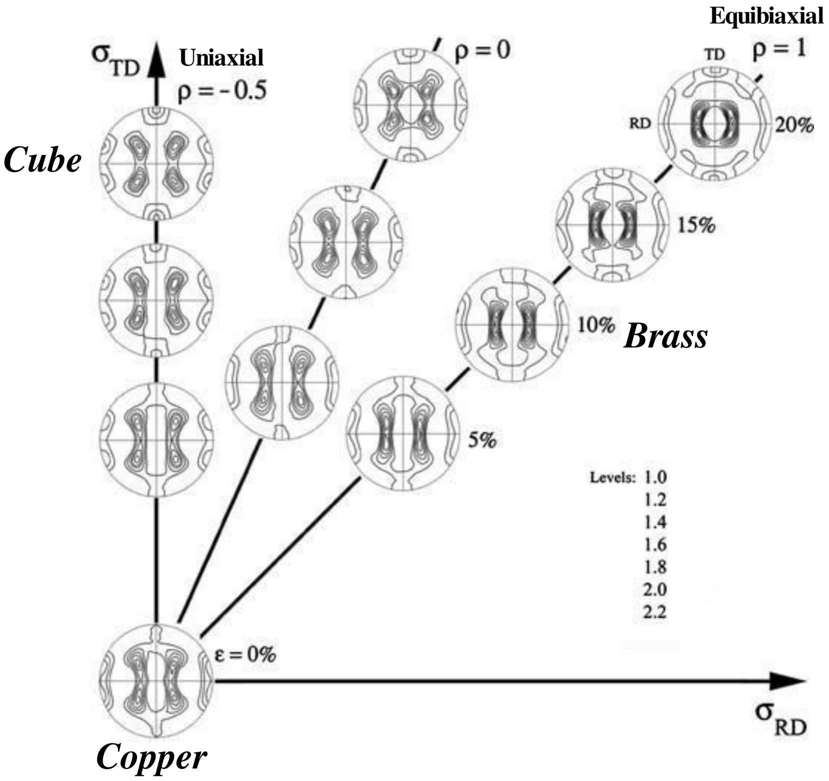

Figure 2.6. Texture evolution of aluminum under various strain paths shown by 111 pole figures [50]

2.2.4. Other textures

One of the important texture components of aluminum is S texture. This texture can be seen after some deformation and it can be seen with Brass and Copper texture [44]. R texture is another common type of texture for aluminum alloys. It can be shown in rolled and annealed sheets, so it is the type of recrystallization texture. The main affecting element for R texture is Fe. PSN texture can also be seen in recrystallized 5xxx and 6xxx aluminum alloys. This texture is important for randomization of the texture for rolling sheets [15]. For some cases in the rolling operation, Goss orientation accompanies strong Brass texture in aluminum alloys [44].

2.3. PLC Effects in Aluminum Alloys

2.3.1. Background

While the metals undergo plastic deformation, their flow behavior can vary according to their composition. For example, carbon containing BCC iron and oxygen containing α-titanium [52] show Lüders bands formation during deformation as shown in Figure 2.7a. For both alloys, solute atoms encircle the dislocation cores in the matrix, so dislocations are pinned by these atoms. Enough high load (or stress) is necessary for the dislocations to maintain their motion. Under sufficient loading, dislocations escape from atmosphere of solute atoms and continue their motion by multiple-cross-slip mechanism [53]. Consequently, mobile dislocation density increases and yielding point decreases for further deformation. If the metal achieves this condition, interruption of loading cannot affect the metal’s homogenous yielding [6].

In some plain carbon steels and aluminum alloys, the serration is not seen only in the yielding region. Due to the continuous interaction between dislocations and solute atoms or other obstacles in the microstructure, the serration behavior is continuous in stress vs. strain curve during deformation as given in Figure 2.7a. Apart from Lüders bands formation in single time, solute atoms diffuse to the dislocations which overcame the solute atoms atmosphere. Therefore, dislocations should again breakaway from solute atoms and this repeated action is called dynamic strain aging.

All in all, the effect result from dynamic aging is called as "Portevin-Le Chatelier" [6]. The detailed mechanism of the PLC effect is explained in Chapter 2.3.2. The major features of the PLC effect are that it is strain rate and temperature dependent and it causes negative strain rate sensitivity (decreasing flow behavior with increasing strain rate) [16].

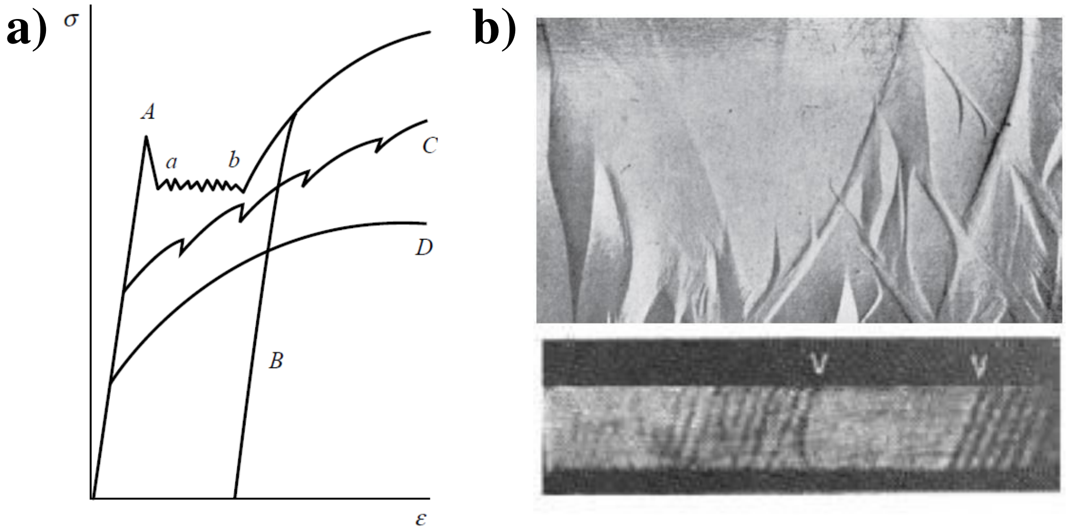

Figure 2.7. a) General stress vs. strain curves of metals (A and B for curve showing Lüders band formation, C for curve showing serrated yielding and D for ordinary hardening behavior) [6] b) surface irregularities after serrated yielding [11,58]

PLC bands (distinct bands) formed owing to PLC effects is one of the plastic instabilities for forming operations. The drawbacks of the PLC bands are:

- Loss of ductility,
- Inhomogeneous deformation,
- Poor surface quality after processes (shown in Figure 2.7b),
- Short fatigue life,
- Undesired stress or strain concentration characteristic,
- Geometrical perturbations,
- Reduced fracture toughness,

- Decrease in effective gauge cross-sectional area and
- More sensitivity to corrosive environments [11,12,33,54–57].

2.3.2. Mechanism

The main underlying mechanism of PLC effect is dynamic strain aging (DSA). At the beginning, there are solute atoms around the lattice of alloys and these solute atoms are inactive at stable conditions. However, at dynamic conditions such as applied deformation, temperature etc. the atoms are activated. At the same time, dislocations start to move in the lattice while deformation increases. The action of mobile dislocations is restricted by the solute atoms or other obstacles (grain boundaries, precipitates etc.). For the shaping operation to be successful, dislocations should continue their motion after critical rate reached. Therefore, dislocations breakaway from the solute atoms. However, due to high diffusivity of solute atoms, they can catch up the dislocations. While deformation continues, mobile dislocations again breakaway from solute atoms and it causes load serrations and strain jumps in the material in macroscopic scale [5–9,16]. In 5xxx aluminum alloys, solute atoms are the Mg atoms. The illustration of DSA is given in Figure 2.8.

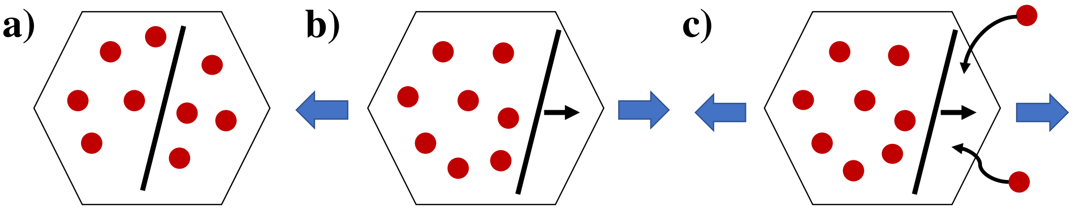

Figure 2.8. Schematic representation of dynamic strain aging showing a) initial unloaded stage b) motion of dislocation under loading c) diffusion of solute atoms to mobile dislocations

2.3.3. Types of PLC bands

Basically, the classification of PLC bands is done as type A, type B and type C according to nucleation and propagation. Type A bands nucleates and propagates continuously in the material until the formation of a new band. Their tensile test curves generally have randomly placed small stress drops during the test [11,59]. Type B bands nucleation and propagation behavior is also continuous with approximately same intervals and their tensile curves are unsteady. Load jumps and drops are higher compared to Type A bands. Finally, type C bands are completely random, they do not have frequency in the nucleation and propagation. Their stress drops can be deeper than type B and type C. The type of PLC bands are strongly affected by strain rate and temperature explained in Chapter 2.3.5.1 [11,32]. All types of PLC bands with their behavior in stress vs. strain curve and tensile specimen are given in Figure 2.9.

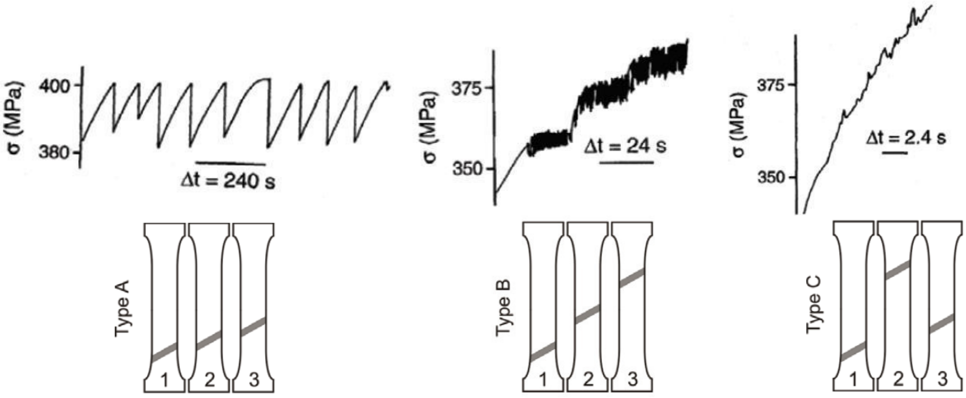

Figure 2.9. Type A, type B and type C PLC bands in stress-strain curve and their motion in tensile specimens [11]

2.3.4. Detection methods

The investigation methods for PLC bands can be classified as optical, thermographic, acoustic, magnetic, electrical and electrochemical [11]. For thermographic analysis, the main principle is detecting the change in the temperature appears from mechanical work and mostly infrared cameras are used for this purpose [60,61]. PLC bands are detected as Figure 2.10a. Since acoustic emission technique is used for the crack detection or for other instabilities (dislocations, twinning etc.), it can be also used for the PLC band observation because PLC bands depend on the dislocation motion.

Magnetic measurements are only for ferromagnetic alloys and it is not applicable for aluminum alloys. On the other hand, electric field measurements related with charge changes between air and metal, electrochemical measurements related with electrolyte (instead of air in electric field case) and metal interfaces in aqueous environment [11].

Among all, widely used method to detect PLC bands is digital image correlation from optical methods. The output of the digital image correlation is strain maps. Since PLC bands localized the strain as a narrow band, the shape of the concentrated strain means PLC band in the strain map. 2D-DIC method is very useful and flexible for in-plane based deformation tests. The basic principle is following the same region with special pattern (i.e. black dots on white surface) in the different pictures and comparing the displacement of these regions with reference picture [62]. By this technique, it is possible to understand the type of the PLC band (Figure 2.10b) [63] (nucleation and propagation characteristic), shape of the band and strain distribution of the band (Figure 2.10c) [64]. Moreover, it is also possible to detect PLC bands from both surface and thickness of the material as shown in Figure 2.10d [65].

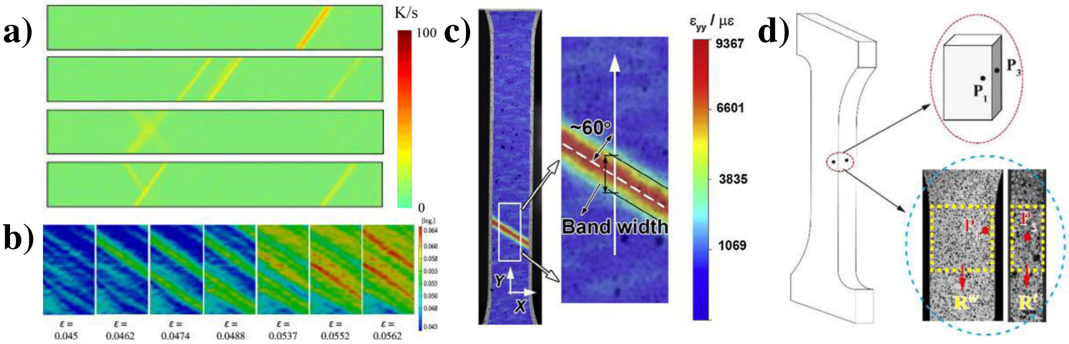

Figure 2.10. a) Detected PLC bands by using thermography [61] b) type B PLC bands detected by DIC [63] c) nucleation and propagation of PLC bands by DIC [64] and d) orthogonal DIC technique for PLC band detection [65]

2.3.5. Factors affecting PLC bands

2.3.5.1. Strain rate & temperature

The most critical factors affecting the PLC band characteristics are strain rate and temperature. These factors not only decide whether PLC bands nucleates and propagates or not, but also decide the nucleation and propagation type of the PLC bands. The typical strain rate and time dependence graphics of 5xxx series of aluminum alloy is given in Figure 2.11a. At higher temperatures, serrations due to PLC effect is suppressed for large range of strain rate. For low temperatures and high strain rates, similarly PLC effect is non-observable. In the area of where serrations are obvious, type of nucleation and propagation of PLC bands again strongly depends on strain rate and temperature and it is given in Figure 2.11b [11]. Also, it is known that:

- Type A bands are evident at high strain rates and low temperatures,
- Type B bands are evident at intermediate strain rates and temperatures,
- Type C bands are evident at low strain rates and temperatures [66].

Another evidence due to PLC bands is the negative strain rate sensitivity. As the strain rate increases, the flow behavior and yielding of the Aluminum alloy decreases [67].

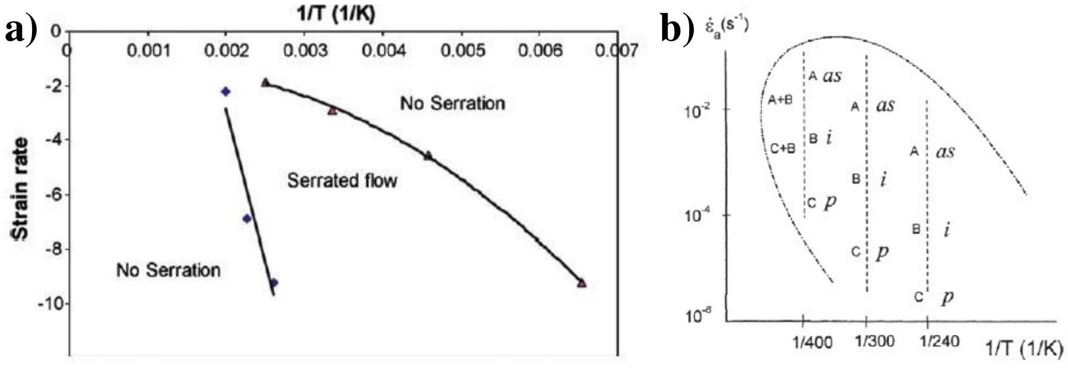

Figure 2.11. Graphs showing temperature and strain rate dependence of a) PLC bands b) types of PLC bands [11]

2.3.5.2. Composition

Solute atoms in the Al-Mg alloys are the main cause of the PLC bands. Their content and other alloying elements in the composition directly affect the characteristics of the PLC bands. For both 5052, 5182 and 5754 aluminum alloys (compositions are given in Table 2.3); serrated yielding and Lüder bands were observed under same deformation conditions. However, the density of serrations in the tensile curves increases with increasing Mg content [68]. Not only serrations, but also the strain distribution in the individual PLC band is also affected by Mg content. Higher strains can be observed in the alloy having higher Mg content. Type C behavior of the PLC bands also manifests itself while Mg content of the alloy is nearly 7% by weight [64].

Table 2.3. Composition of different 5xxx series of aluminum alloys [68]

Alloy	Mg	Si	Fe	Cu	Mn	Cr
5052	2.470	0.196	0.472	0.032	0.075	0.203
5182	4.351	0.084	0.218	0.044	0.316	0.011
5754	2.854	0095	0.239	0.028	0.316	0.011

For different series of aluminum alloys such as 2xxx and 7xxx, it is well known that major alloying elements in these alloys (copper and zinc, respectively) have weak effect on the formation of PLC bands. The main reason is the lowest mismatch values than Mg atoms. In 7020 alloy, even if presence of Mg atoms contributes to the PLC action, it is not well-pronounced compared to 5082 aluminum alloy [67]. The differences in the serrations from stress vs. strain curves also increases with the increasing Mg or Zn content in aluminum alloys [69].

2.3.5.3. Microstructure & second phases

Grain boundaries and second phases are the pinning sites for the dislocation motion and PLC bands are based on the dislocation motion. Each features of microstructure should be very effective for PLC bands. Since microstructure and second phases can be controlled by the deformation processes or heat treatments, this chapter also includes the effect of these parameters. The heat treatment of Al-Mg alloys causes the decrease in dislocation density and pre-strain. However, heat treatment increases the vacancies in the lattice, so mobility of solute atoms increases. As a result, higher diffusion coefficient of Mg atoms causes faster locking. Faster locking also means increase in amount of load jump and drops [70]. Breakaway action of mobile dislocations from solute atoms are also easier in the sample having large grains and it increases the load jumps and drops. Severe serrations can be observed in the deformed (hot and cold rolled) samples compared to annealed samples because of high number of dislocations and grain boundaries [69,71,72]. Additionally, PLC band propagation velocity is also higher in the alloy having larger grains than smaller grains. Especially the alloy having fine grains i.e. severely deformed have the lowest velocity of PLC bands. The type of PLC bands become more complex while grains are getting finer. For coarse grains, the PLC type is type A and for fine grains, it is type A, B and D together [14]. Instead of annealing heat treatment, quenching heat treatment can result in suppressing of serrations under lower strain rates (10^{-5} s^{-1}). For higher strain rates (10^{-4} s^{-1}), the PLC action is observed later in quenched samples than annealed samples [21].

The main second phase of the 5xxx series of aluminum alloys is the Mg_2Al_3 intermetallic. Higher annealing times (100 h) at recrystallization temperature results in coarser particle size of these phases as shown in Figure 2.12. Higher annealing times decreases the Mg solute atom concentration by creating coarser precipitates and PLC bands can be formed continuously. Continuous propagation of PLC bands means type A behavior [20]. Nano-scaled precipitates can be also a factor for changing the nucleation and propagation characteristic of Aluminum alloy. While it is expected that, PLC band propagation starts with continuous and continue with hopping propagation; in the alloy having nano-scaled precipitates, the type of the PLC band is A, B or C without transition during the testing [73].

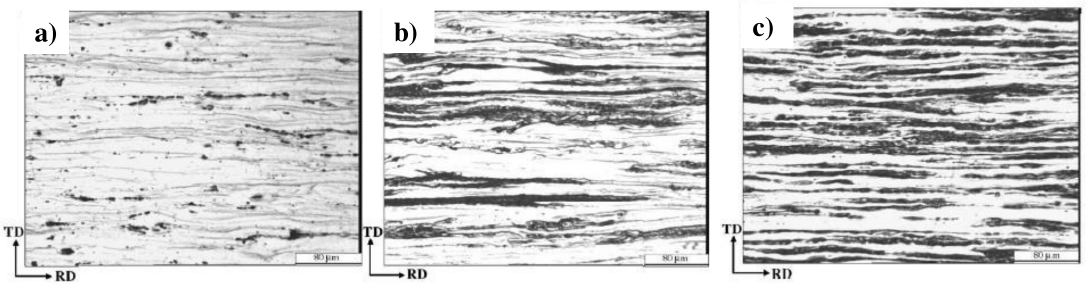

Figure 2.12. Microstructures of 5182 aluminum alloy a) as received and after annealing of b) 182°C for 30 h c) 182°C for 100 h [20]

2.3.6. PLC effect under various strain paths

To achieve various strain paths, one of the methods is the changing the shape of the specimen. Creating the notches on round tensile test specimen (shown in Figure 2.13a) can change the stress triaxiality ratio of the deformation processes. While serrated flow of the tensile specimens with notches show suppressed behavior with the direction of 45° and 90° to the rolling axis, serrated flow is detected for all tensile test specimens parallel to rolling direction as shown in Figure 2.13b [22]. For sheet samples, it is also possible to reach plane strain condition by creating the notches on the specimen [34]. Under plain strain condition, the PLC bands are less obvious than under uniaxial condition in the strain maps obtained from DIC method.

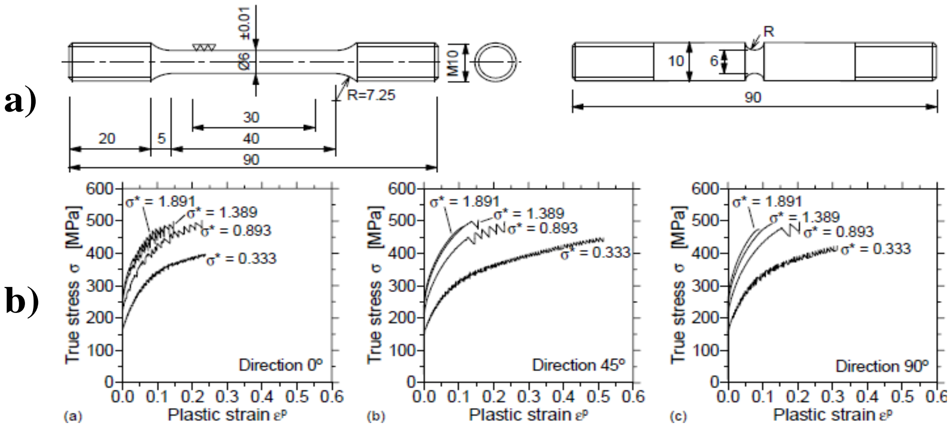

Figure 2.13. a) Notched round tensile test specimens to achieve various strain paths b) stress-strain curve results of these specimens [22]

The other strain path studied in the literature is shear strain path [74]. Under the shear loading, the PLC effect is again observable and for reverse loading under shear setup, the PLC orientation changes according to loading direction.

Deformation characteristics of aluminum alloys are commonly studied under biaxial condition in the literature. Purpose of these studies can be about forming characteristics (i.e. obtaining forming limits, fracture limits, yield loci) or about PLC bands of aluminum alloys.

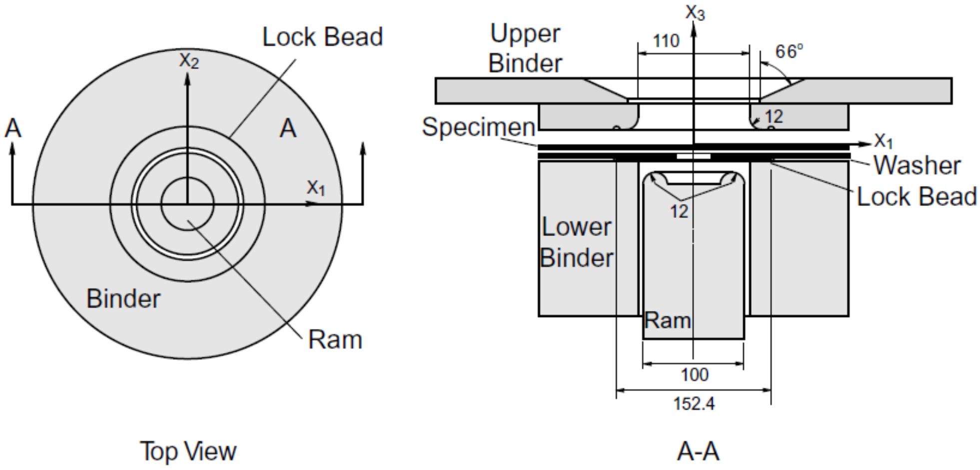

Figure 2.14. Schematic of Marciniak test machine [75]

Mostly used methods to achieve equibiaxial or plane strain conditions are Marciniak (shown in Figure 2.14) or hydraulic bulge testing. By using Marciniak testing, it is possible to reach stress vs. strain curves to understand the forming characteristics of the 5xxx series of aluminum alloys. Figure 2.15a shows the one of the curves of 5754 aluminum alloy under annealed condition, these curves indicate the stress and strain values of rolling direction and transverse direction. The purpose was matching the experiment results and some models such as von Mises', Hill'48, Hosford'79 and Yld2000-2d model shown in Figure 2.15b [75]. Additionally, strain values in both x and y direction (major and minor) during testing of 5754 alloy for rolling direction and transverse direction was plotted by Iadicola et al. [27] under various strain paths (Figure 2.15c). In this case, the purpose was collecting data for crystal plasticity model. Other study of Marciniak testing of 5xxx series of aluminum alloy [51] is about investigating the microstructure and texture. Initial polished surface of the material became rough by forming grooves parallel to rolling direction after some strain levels (>0.2). This roughening was related to crystallographic texture of the material and higher {220} components of the texture resulted in more roughening of the surface in macro scale. Nonetheless, this study has no information about presence of PLC bands.

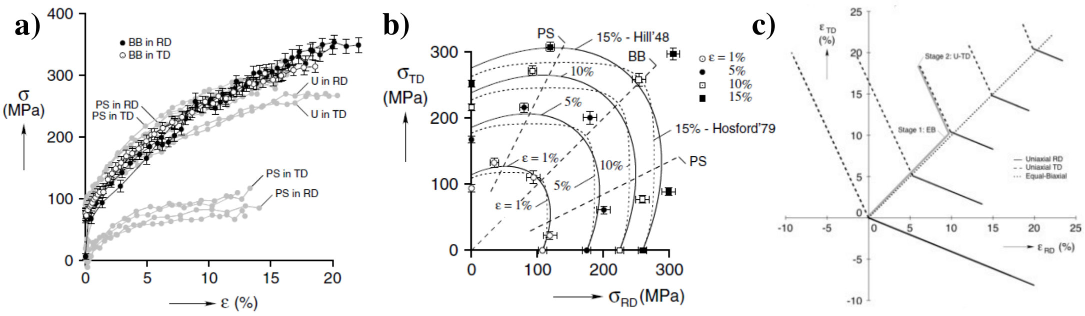

Figure 2.15. a) Stress vs. strain curves of 5754 aluminum alloy under various strain paths by using Marciniak testing b) comparison of some mechanical models with Marciniak test results [75] c) strain in x direction vs. strain in y direction graph under various strain paths [27]

For hydraulic bulge testing; apart from PLC bands in the uniaxial condition, instabilities were categorized as localized deformation ring (LDR), localized deformation circle (LDC) and localized deformation band (LDB). These instabilities were detected by digital image correlation technique. The first observed instability was LDR and strain was localized in the ring, so it became LDC. Lastly, formation of LDB was observed at angle of 0°, 45° and 90° to the transverse direction and the behavior of the band is similar to type C PLC bands [25]. The spatial analysis of these instabilities is given in Figure 2.16.

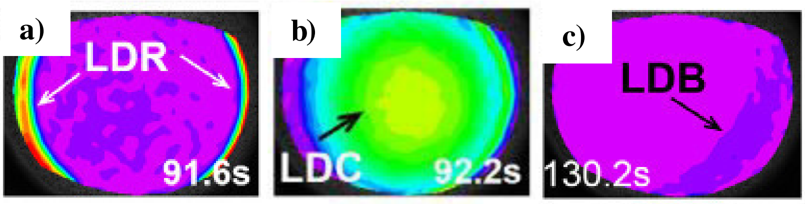

Figure 2.16. Some plastic instabilities of 5754 aluminum alloy a) localized deformation ring b) localized deformation circle c) localized deformation band under biaxial condition [25]

The other type of testing used for biaxial loading condition is cruciform testing. This testing is also used to understand the forming characteristics by yield loci similar to Marciniak testing for 5xxx series of aluminum [26]. Spatio-temporal analysis with the help of digital image correlation to detect strains for cruciform testing was also used in the literature under various strain paths and results showed that the type of PLC bands changed according to stress states. Serrations under uniaxial conditions changed from type A to type B while it is near to type B under plane strain condition. Also, it is stated that yielding behavior of the aluminum was not affected from the strain path changes [30]. Digital image correlation for cruciform testing is also chosen to investigate the forming limit strains and one of the strain-time plot is given in Figure 2.17a. [29].

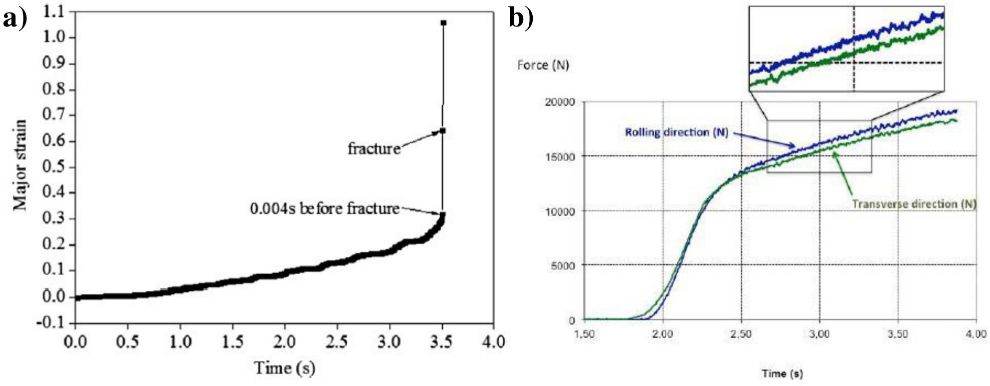

Figure 2.17. a) Strain-time plots [29] b) load-time plots [76] of aluminum alloys showing PLC bands under biaxial condition

Although above all mentioned studies for various strain paths investigated the 5xxx aluminum alloys, literature has lack of studies about some properties of PLC bands such as velocity, nucleation, propagation, shape etc. The first study of spatio-temporal analysis of individual PLC band was done by using both digital camera (for DIC) and infrared camera equipped to cruciform testing setup [76]. Analysis of heat source map created with the help of infrared camera gave the shape of individual PLC band. Effect of PLC bands on the loading response with respect to time was also studied and load jumps and drops are clear as shown in Figure 2.17b. The cross over characteristic of PLC bands for different strain paths was also studied with the same setup and it was stated that morphology of PLC bands strongly depends on stress state. The action of PLC bands can be summarized as;

- Under uniaxial condition, bands nucleated and propagated with the exact angle to the loading axes,
- Under plane strain condition, this action is perpendicular to the major loading axis,
- Under equibiaxial condition, nucleation and propagation actions have a shape of "X" [77]. These actions are given in Figure 2.18.

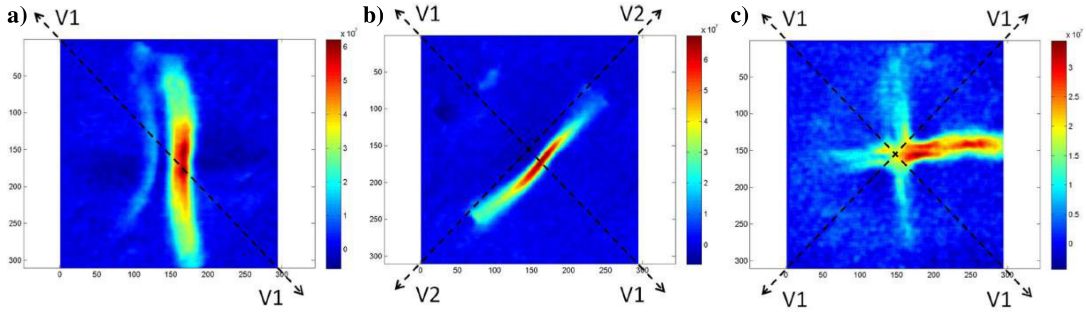

Figure 2.18. PLC band propagation under a) uniaxial loading b) plane-strain loading c) equibiaxial loading [77]

2.4. Critical Review of the Literature

The strengthening mechanism of 5xxx series of aluminum alloys are known as solid solution strengthening and strain hardening. However, in the literature, the studies focused on these mechanisms are separated. Since texture is one of the most critical parameters for strain hardening mechanism, there are many studies to examine the final texture after deformation processes. On the other hand, for solid solution strengthening, one of the critical parameters is PLC bands. In the literature, spatio-temporal analysis of the PLC bands is most widely studied and microstructural parameters (grain size, second phases, etc.), temperature, strain rate were mostly preferred parameters to affect PLC bands. Among affecting parameters, strain path change was not commonly chosen. Although there are few studies under different strain paths, these studies just focus on the anisotropic behavior, yield loci, forming and fracture limits and nucleation or propagation characteristics of the PLC bands. Variation of texture and fracture characteristics under PLC bands based deformation are still gap in the literature. Additionally, two different strengthening mechanism of this alloy with critical parameters (texture and PLC bands) are studied together in this work.

CHAPTER 3

EXPERIMENTAL PROCEDURE

3.1. Initial Material

The initial material was commercially produced Aluminum 5754-H111 alloy. The alloy was determined by optical emission spectroscopy. The chemical composition of the alloy is given in Table 3.1 which proves that magnesium content (2.88%) of the supplied aluminum alloy is appropriate for 5754 designation. It was received in the form of rolled-sheet having 2 mm thickness, 1000 mm width and 2000 mm length.

Table 3.1. Weight percentages of elements in 5754 aluminum alloys

Al	Mg	Fe	Si	Mn	Zn	Cu	Sn	Ti	V	Ga
Balanced	2.88	0.4	0.39	0.14	0.1	0.06	0.03	0.02	0.02	0.01

Examining the microstructure of 5754 aluminum alloy with solution etching is difficult due to advance corrosion resistance characteristics of alloy. Solution containing 30 ml HCl, 70 ml HNO_3, 10 ml HF, 4g Cr_20_3 and 240 ml distilled water reveals few grains and there are some undesired etching pits in microstructure as shown in Figure 3.1a. Imaging unit was Huvitz HDS-5800 series. Before solution etching, standard metallographic sample preparation procedures were applied to the material which includes cutting, molding, grinding and polishing with diamond paste. To obtain more precise microstructure i.e. manifest grains and grain boundaries, Electron Backscattered Diffraction (EBSD) method was used after electropolishing. Details of the EBSD sample preparation and data collection procedures is mentioned Section 3.2. The microstructure of material achieved with EBSD shown in Figure 3.1b. Average grain size measurement was done on this micrograph by using method of Heyn Lineal Intercept Procedure mentioned in ASTM E112-13 [78]. As a result, the material had uniform microstructure with an average grain size of 10.3 ± 1.3 μm.

Since H111 designation means some amount of cold working just after annealing [2], calculated grain size verifies this designation.

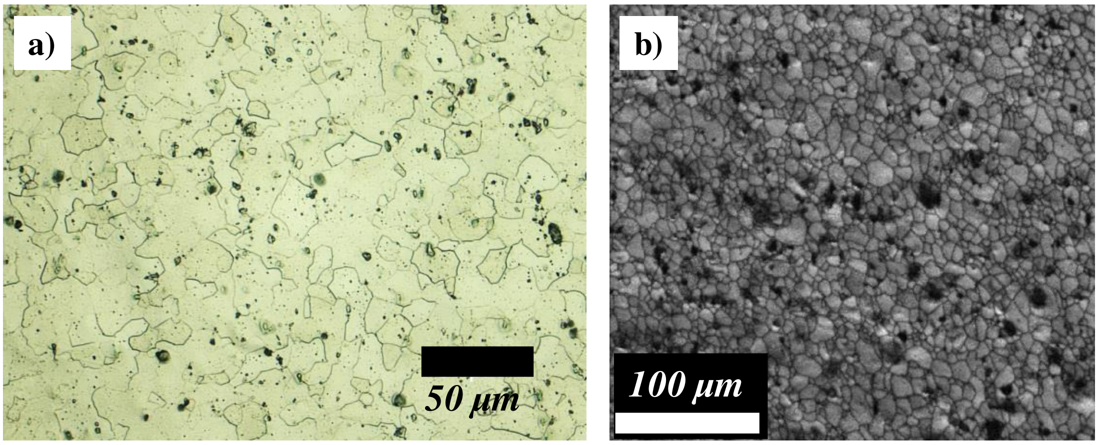

Figure 3.1. Microstructure of the as-received aluminum sheet obtained from a) optical microscopy b) EBSD

Hardness of the material was measured with Shimadzu HMV-2 Microhardness Testing System after polishing operation. Applied load in the system was fixed to 0.5 kg and different sections of the sheet was used as a sample. Hardness of the material taken from the surface was 62.2 ± 2.1 kg/mm^2 and homogenous along the sheet. At least 10 different hardness measurements were taken from each sample.

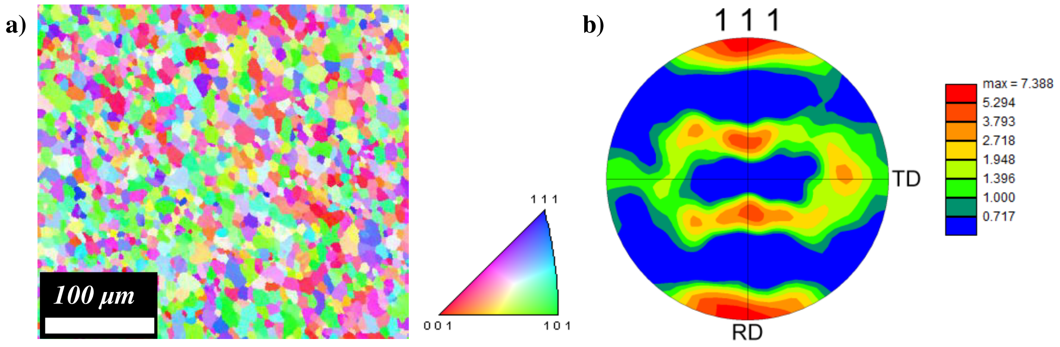

Figure 3.2. EBSD analysis of as-received aluminum sheet showing a) grain orientation map b) 111 pole figure

Since this work includes the discussion of texture change during the deformation, texture analysis of the initial sample was done with EBSD. Figure 3.2a and 3.2b shows the orientation of each grain and 111 pole figure of the microstructure of material shown in Figure 3.1b, respectively. Therefore, material initially had Copper type of texture which is typical of rolled aluminum sheets. Copper texture means material having deformed grains and fine dispersoids after final cold rolling [47].

3.2. SEM & EBSD Analysis

FEI Nova Nano SEM 430 field emission scanning electron microscope at 18 kV accelerating voltage was used to monitor the surface irregularities, defects, slips and micro cracks after testing and to analyze fracture surfaces. The material was failed mostly with the shape of cross to the loading directions and fracture surfaces were placed to the stage of SEM perpendicular to gun position. For surface irregularity analysis, pit region was directly examined after rinsing and drying with ethyl alcohol or acetone.

EDAX EBSD camera equipped to SEM obtained the diffraction data with the software of Orientation Imaging Microscopy (OIM) Data Collector. Figure 3.9 shows the sample, sample holder and camera position in SEM. As it can be seen from figure, sample holder has a 70° angle for EBSD camera to collect electrons. Voltage, working distance and spot size values were set to 25 kV, 10 mm and 5 respectively for better electron collection. OIM Analysis software was used to plot orientation maps and pole figures.

To obtain texture and grain orientation of initial material, 2 µm step size was used. Larger areas such as 450x450 μm^2 (approximately 2000 grains) were studied for the representative pole figures for deformed samples with same step size with initial materials. Since shear bands are narrow surface irregularities, examined area was 50x50 μm^2 and steps size was fixed to size of nanometers. Standard cleanup procedures were applied in this software for larger areas. For small and much deformed areas, unreliable data were ignored and showed with black color. Sample preparation for EBSD was done with the electropolishing parameters and solution given in Section 3.5.

3.3. Rolling and Annealing Experiments

3 x 5 cm^2 samples were cut from 2 mm thick as-received sheet with metallographic abrasive cutter for rolling experiments. Rolling were done by using OAM Cavallin M120 laboratory scale mill (roll diameter: 65 mm). Deformation rate and roll speed of the mill are 3.5/s and 32 m/s, respectively. For cold rolling experiment, final samples have reduction of thickness values of 33% and 66%. For 33% rolling, three passes were chosen to prevent the material from unexpected failures. For 66% rolling, the final sample was produced with seven passes. For hot rolling experiments, custom-made furnace temperature was set to 480°C and the materials were annealed for 5 minutes just before the operation with single pass. Although chosen percentages of reduction in thickness is less than percentages used in the industry, it is necessary to reduce industrial percentages to obtain different kind of textures.

For annealing after rolling, temperature was chosen according to recommendation of ASM. 345°C for 1.5 hours were applied to the samples after hot and cold rolling. Additional annealing to detect abnormal grain growth was also applied. For this detection, 510°C was chosen and annealing time was changed.

3.4. In-plane Biaxial Testing

The portable biaxial testing apparatus was assembled to a Shimadzu Bending Test Machine (capacity of 10kN) given in Figure 3.3a. This apparatus has capability to be used in uniaxial, equibiaxial, in-plane stretching and compression. Apparatus converts the vertical load to horizontal loads along four independent arms (one of them shown in Figure 3.3b). Horizontal loads can be controlled by changing the θ angle shown in Figure 3.3b. Vertical load was always known in bending test machine and horizontal load acting on each arm were calculated by Equation 1:

$$F_{horizontal} = \frac{F_{vertical} * \tan\theta}{4} \tag{1}$$

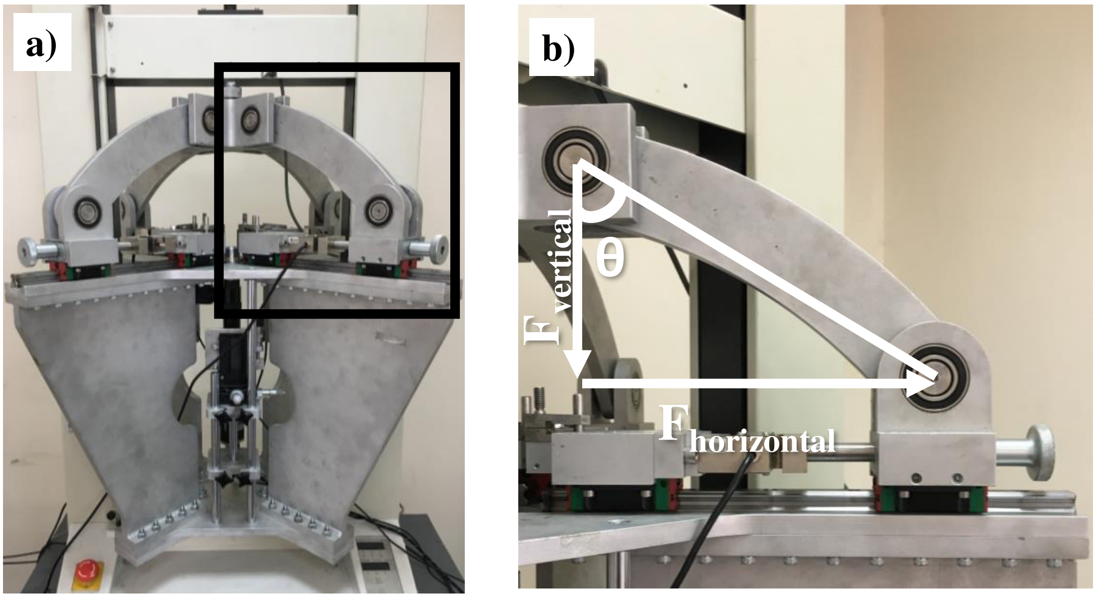

Figure 3.3. a) Portable biaxial testing apparatus assembled to test machine b) closed view of one of the arms shown in black rectangle in apparatus

Arms have same length to distribute the forces equally as shown in Figure 3.4. Load cells recording data every 6 sec were attached to the arms and load difference at each arm does not exceed 100 N during the test. For uniaxial testing, two arms of the specimen along the rolling direction ($F_2 = F_4 = F_{horizontal}$, $F_1 = F_3 = 0$) were attached to the apparatus whereas for equibiaxial testing, all arms of the specimen were attached ($F_1 = F_2 = F_3 = F_4 = F_{horizontal}$). For attachment, sample holder with jaw grips and screws were used. Strain rate was always kept at 0.5 1/s for both loading conditions.

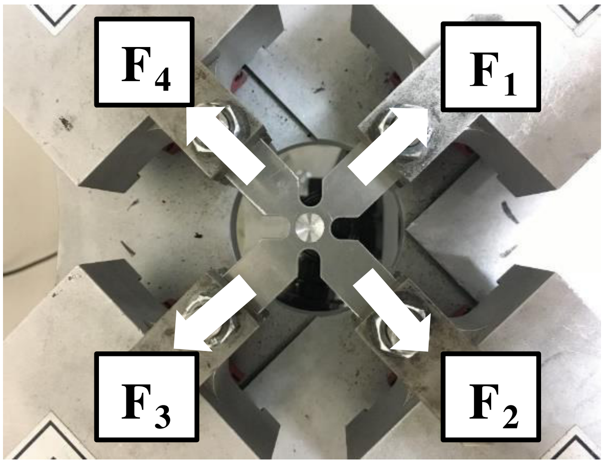

Figure 3.4. Acting forces on the specimen attached to the biaxial testing apparatus

3.5. Cruciform Shaped Specimen

Cruciform shaped sample used in testing was cut by water-jet from the rolled sheet and geometry of the sample is given in Figure 3.5. The design of the specimen has symmetrical shape and has four notches in the middle region. Additionally, specimen has pit in the middle to localize strain in desired region. Strain localization method can be called "reduced cross section". Detailed design procedure can be found elsewhere [79].

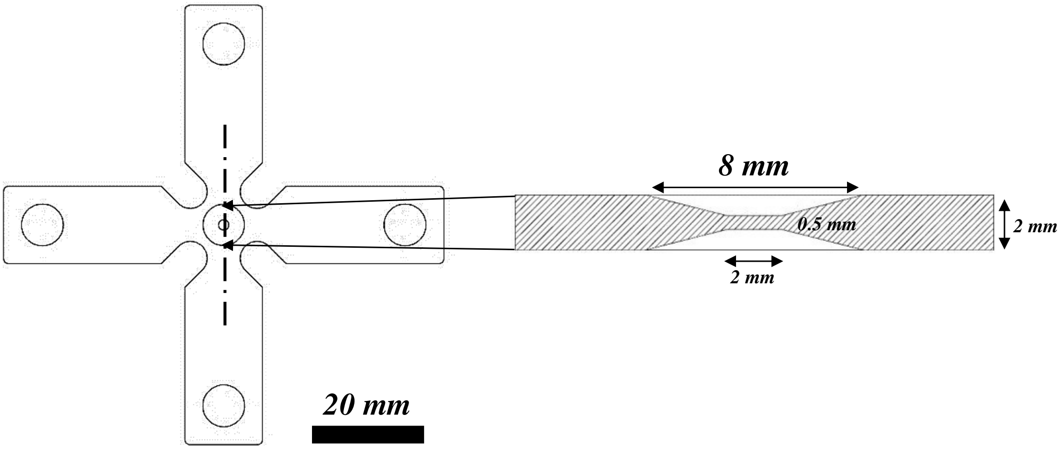

Figure 3.5. Geometry of the cruciform shaped specimen

CNC milling (HAAS VF-1 CNC Vertical Milling Machine) was used to obtain this region. The machine has three-axes. HSS (with Cobalt addition) cutting tool with a shape of truncated cone for this operation was specially manufactured. Because of the small size of the pit, the tolerance of the milling operation should be minimized. For this purpose, special sample holder was manufactured also. After milling operation, thickness of this region has a smooth transition from 2 mm to 0.5 mm. The diameter of the region is also reduced from 8 mm to 2 mm. Measured roughness value by Mitutoyo SURFTest SJ-400 profilometer was approximately 1.5 µm. However, the roughness needed more reduction and electropolishing was done on the pit region.

The pit region was electropolished with Struers Lectropol-5 device with Struers A2 solution (90 ml distilled water, 730 ml ethanol, 100 ml butoxyethanol and 78 ml perchloric acid). Electropolishing was done at 38 Volts for 30 seconds. It is one of the best methods for polishing the samples having complex geometries. Purpose of electropolishing was not only to reduce the surface roughness but also eliminate the surface irregularities formed during milling. Figure 3.4 shows the differences in the surface of pit region after each preparation stages.

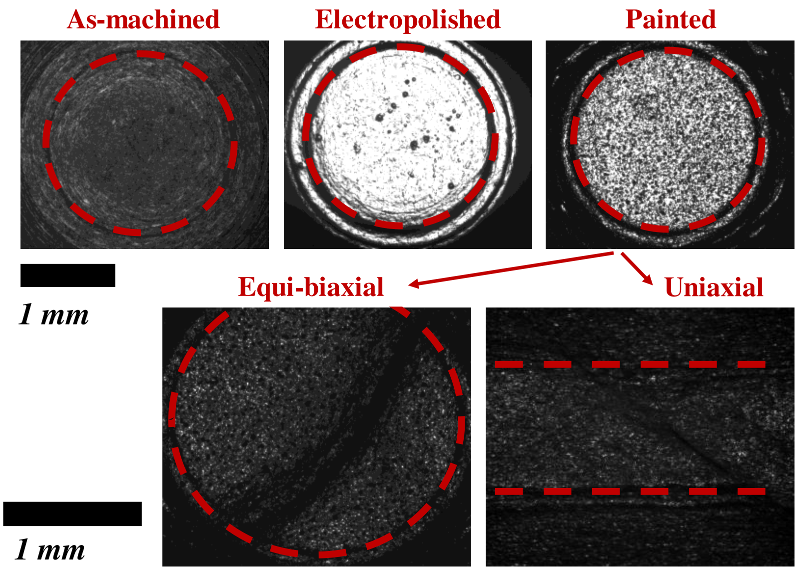

Figure 3.6. Image of pit region's surface after preparation steps and applied deformation

3.6. Digital Image Correlation

Digital image correlation setup (Figure 3.7) consists of Basler piA2400-17gm GigE camera (5 MP resolution) with Sony ICX625 CCD sensor, Navitar Ultra Zoom 6000 zoom lens (1.40X-9.00X and NA=0.023-0.071, respectively) with co-axial LED illumination and 2X adapter, and a manual microstage. The setup was placed under the cruciform specimen in order to monitor the 2 mm diameter pit (middle) region of the cruciform sample. 2.9x2.2 mm^2 field-of-view was obtained at 1.4X magnification with 2448x2050 pixels resolution. Acrylic paint (diluted with acetone) was sprayed to the monitored region with airbrush for these magnifications. Spraying achieved the proper speckle pattern and contrast for DIC with average 25 μm black speckles on electropolished shiny surface. The recording rate varied from 1 fps (for spatial analysis) to 5 fps (for temporal analysis). Purpose of the higher fps values was achieving higher strain resolutions and obtaining more precise strain jumps.

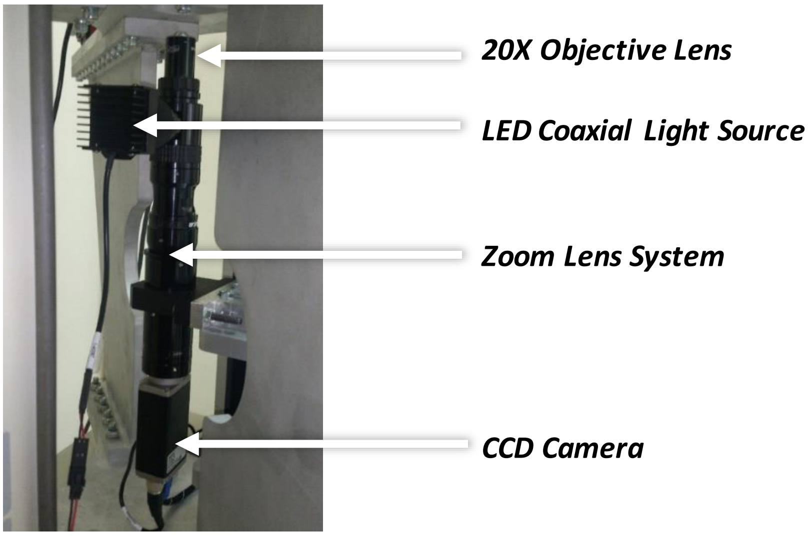

Figure 3.7. DIC imaging unit with its indicated components

Matlab based 2D digital image correlation software Ncorr v1.2 [80] was used to analyze strain distribution of the monitored region. This software is based on just mathematical correlation. Strain resolutions were 1.08 µm and 5.05 µm for 3X and 1.4X magnification, respectively. This resolution was adjusted by changing the subset size in the software. Error calculated by translation experiments was 0.14% for these magnifications. All images recorded with 5 fps rate were used to obtain strain-time graphs whereas consecutive images recorded with 1 fps rate were used to obtain spatial analysis of PLC bands. For spatial analysis, strain maps from the DIC software output were evaluated. Example of the DIC result is given in Figure 3.8 to illustrate the spatial and temporal analysis.

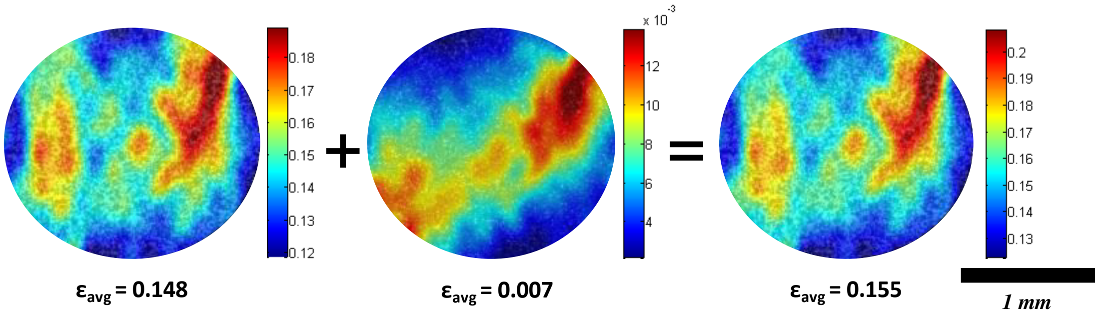

Figure 3.8. Overall DIC results (strain map) of two consecutive images and strain map between these images during testing

Median strain values from output of the program at each time interval were collected to plot strain-time graphs. Software calculated strains as Green-Lagrangian strains in x and y direction and they were converted to the true strain with the Equation 2:

$$\boldsymbol{\varepsilon} = \boldsymbol{ln}(\sqrt{\mathbf{2}\boldsymbol{E} + \mathbf{1}}) \qquad \textbf{(2)}$$

where ε is true strain and E is Green-Lagrangian strain.

Moreover, equivalent strain calculation was done by Equation 3:

$$\boldsymbol{\varepsilon_{eq}} = \sqrt{\mathbf{2/3}(\boldsymbol{\varepsilon_{xx}}^{\mathbf{2}} + \boldsymbol{\varepsilon_{yy}}^{\mathbf{2}} + \boldsymbol{\varepsilon_{zz}}^{\mathbf{2}})} \qquad \textbf{(3)}$$

While DIC software can give strain results in xx and yy direction, strain in thickness was obtained by assuming that summation of strains in three axes equals to zero.

For true stress measurement, actual load was divided to actual assumed area. Assumption was based on adding elongated area to initial thickness reduced area shown in Figure 3.3. The calculations were done by Equation 4:

$$\sigma_{true} = \frac{F}{initial\ area\ (7.5\ mm) + (\varepsilon_{zz} * \varepsilon_{xx\ or\ yy})} \tag{4}$$

F is load and σ is stress. Equivalent stress was measured by Equation 5:

$$\sigma_{eq} = \sqrt{\frac{(\sigma_{xx} - \sigma_{yy})^2 + (\sigma_{xx} - \sigma_{zz})^2 + (\sigma_{yy} - \sigma_{zz})^2}{2}} \tag{5}$$

CHAPTER 4

INVESTIGATION OF TEXTURE & MICROSTRUCTURE OF 5754 ALUMINUM ALLOY

4.1. Deformation Textures & Microstructures

4.1.1. Cold working textures & microstructures

After deformation of aluminum alloys with 33% thickness reduction, formation of slip bands in deformed grains is obvious as seen in Figure 4.1a. Elongation of few grains is clearly observed. On the other hand, it can be stated that 33% deformation does not cause significant change in the texture which is typical copper texture before and after the deformation (Figure 4.1b).

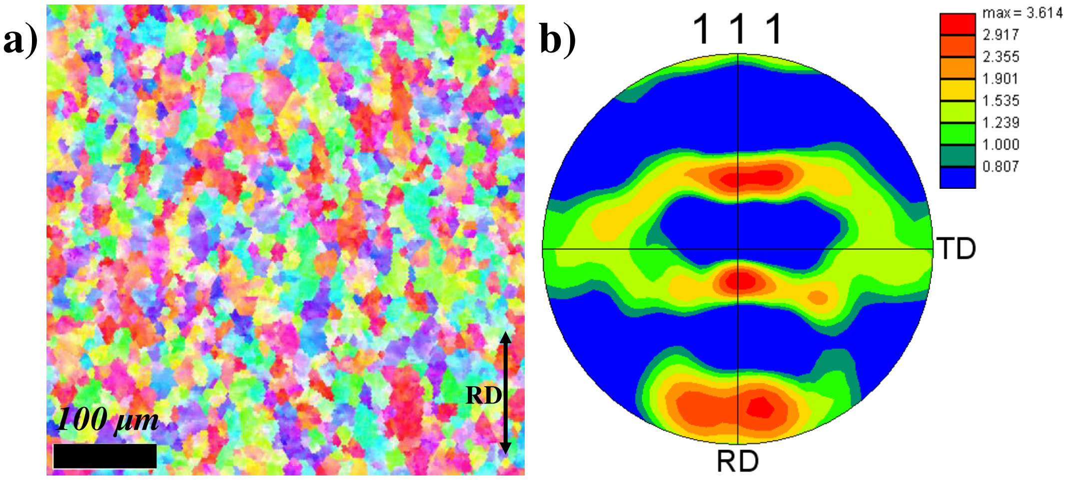

Figure 4.1. a) Grain orientation map b) 111 pole figure of 5754 aluminum alloy after 33% cold rolling

Secondly, elongation of more grains with more slip bands is seen in 66% deformation by rolling operation as shown in Figure 4.2a. Similar with 33% deformation case, the texture is typical rolling texture (Figure 4.2b). Intensity of {101} (green color in grain orientation map) is higher than 33% case. Brief description of this kind of textures is propagation of {112}<111> orientation through {123}<412> and {110}<112>.

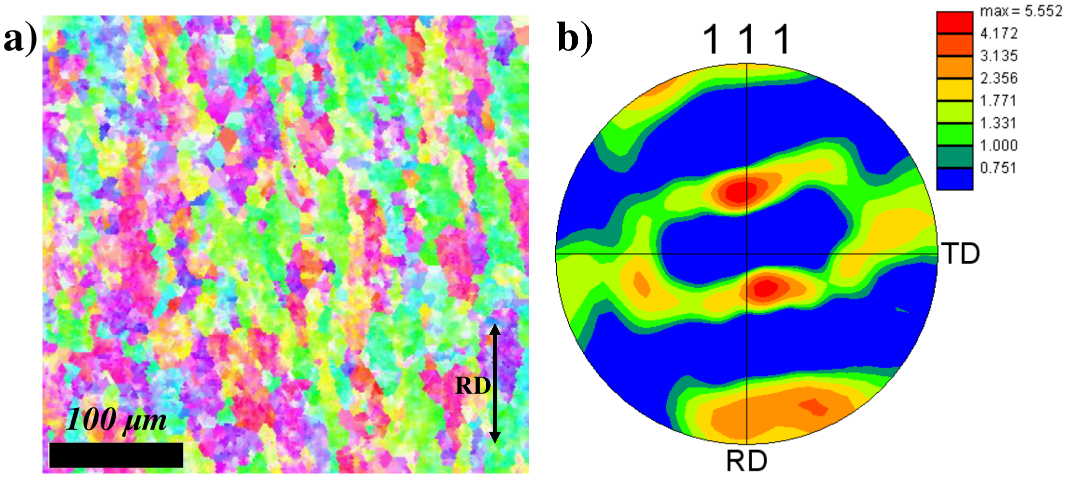

Figure 4.2. a) Grain orientation map b) 111 pole figure of 5754 aluminum alloy after 66% cold rolling

4.1.2. Hot working textures & microstructures

For hot rolling, the temperature was chosen as 480°C and reduction in thickness is 33%. The overall result is increase in copper type of texture component as shown in Figure 4.3a. Intensity of the region that represent the copper texture also increased. Although hot rolling texture component is observed as cube texture in the literature [47], examined texture in this study shows that for small amount of reduction in thickness, hot rolling results in formation of brass texture in Al-Mg alloys. When compared to 33% cold rolled structure, there are small deviation from copper texture for hot rolling (Figure 4.3b).

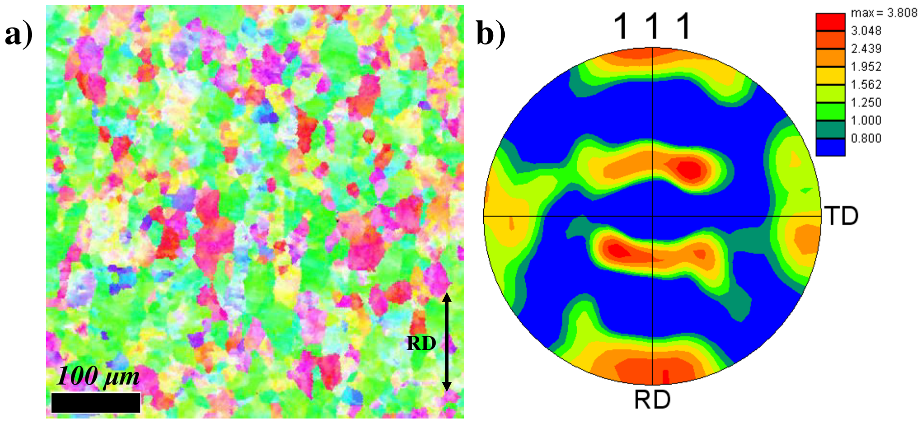

Figure 4.3. a) Grain orientation map b) 111 pole figure of 5754 aluminum alloy after 33% hot rolling

4.2. Annealing Textures & Microstructures

Annealing textures include the texture of annealed materials after rolling mentioned in Chapter 4.1 (different amounts of cold rolling and hot rolling). Annealing temperature and time were 345°C and 1.5 hours, respectively.

First of all, 33% cold rolled aluminum alloy has a microstructure of equiaxed grains and it is observed that recrystallization is completed for given annealing temperature and time (Figure 4.4a). For pole figures given in Figure 4.4b, the 33% cold rolled texture is prevented, there is no significant change after annealing operation. The texture is typical cold rolling texture which is known as copper.

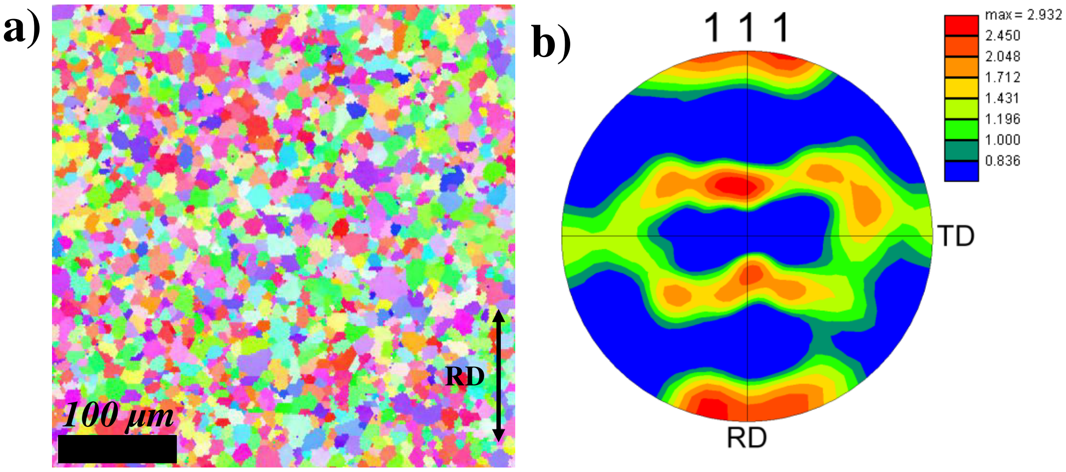

Figure 4.4. a) Grain orientation map b) 111 pole figure of 5754 aluminum alloy after recrystallization of 33% cold rolling

The shape of grains for 66% deformed and annealed material is fully recrystallized equiaxed as shown in Figure 4.5a. It is higher than 33% case. Annealing texture of 66% deformed aluminum is slightly different from that of 33% deformed. For texture, cube components are seen from Figure 4.5b. These components are not so sharp but it can be concluded that higher deformation amounts promote the formation of cube texture. The reason behind this can be creation of more nucleation sites after higher deformations for cube components.

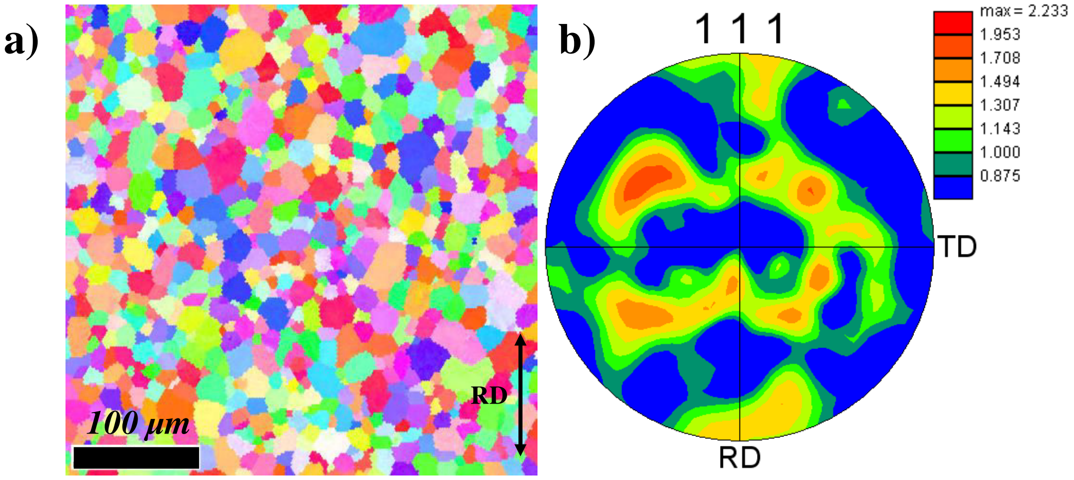

Figure 4.5. a) Grain orientation map b) 111 pole figure of 5754 aluminum alloy after recrystallization of 66% cold rolling

Annealing parameters mentioned above causes the full recrystallization of grains after 33% hot rolling operation like cold rolling. Grains have equiaxed shape after heat treatment operation as it can be seen from Figure 4.6. Texture is not affected by annealing operation, brass texture is again seen in the pole figure.

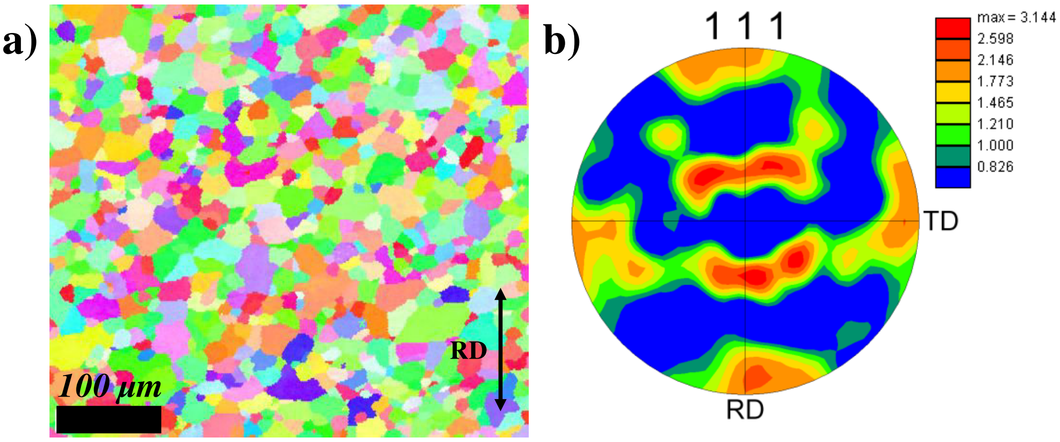

Figure 4.6. a) Grain orientation map b) 111 pole figure of 5754 aluminum alloy after recrystallization of 33% hot rolling

4.3. Abnormal Grain Growth

At 510°C, abnormal grain growth of the 5754 aluminum alloys after relatively short time intervals is clearly observed from microstructures given in Figure 4.7. 3 minutes of recrystallization at that temperature results in fully recrystallized grains whose average diameters are 9.9 ± 3.9 µm (Figure 4.7a). Abnormally grown grains do not exist in the microstructure. However, for 10 minutes at that temperature results in growth of specified grains in the microstructure (shown in Figure 4.7b). This motion of abnormal grain growth seems to be discontinuous and growing grain consumes the adjacent smaller grains. The reason behind the abnormal grain growth is absence of particles responsible for pinning action due to dissolution of second phase particles in the matrix.

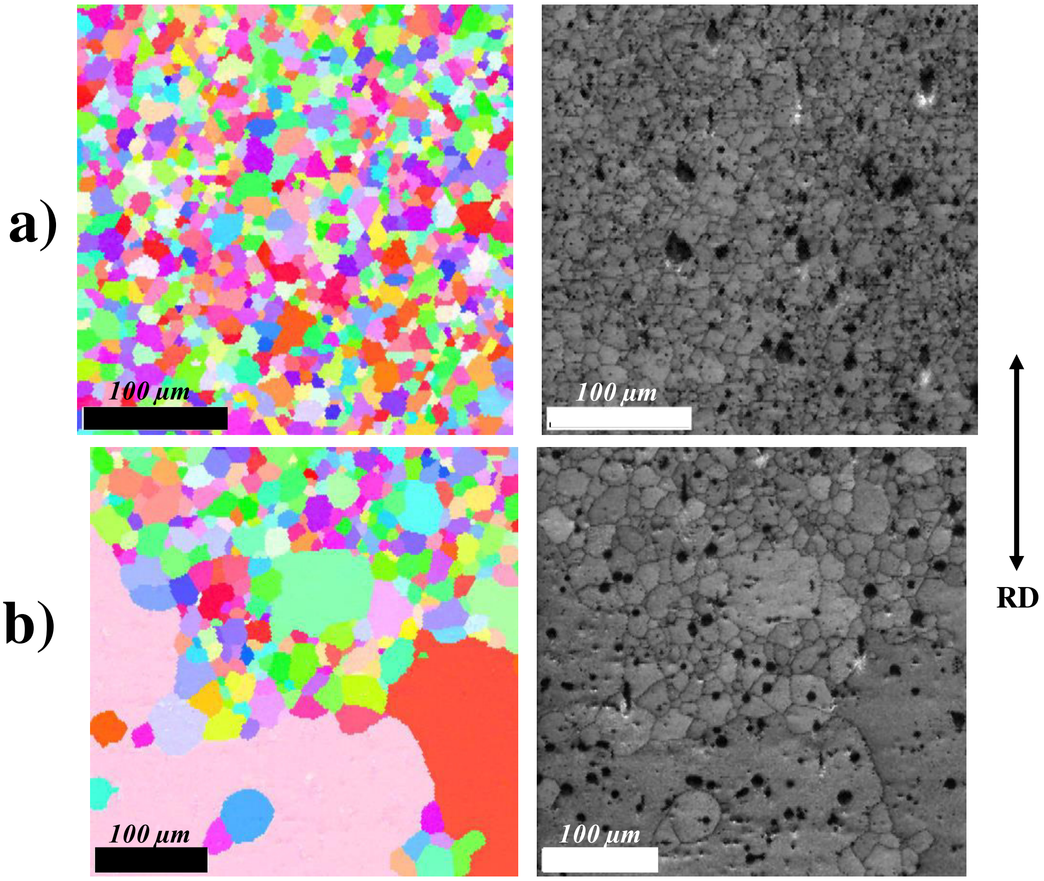

Figure 4.7. EBSD results of the material after a) 3 minutes of annealing b) 10 minutes of annealing at 510°C

For texture, it can be stated that for lower annealing times at high temperatures (with no grain growth) do not cause change in the general texture of the material. Copper texture after 33% cold rolling is maintained just like the case of 345°C for 1.5 hours. For longer times for annealing, grains which are abnormally grown have the component of {100} and {110} family. On the other hand, {111} component tends to decrease. The overall results of texture experiments are given in Table 4.1.

Table 4.1. Summary of the formed texture after experiments

Rolling	Reduction in thickness	Annealing	Texture result
Cold	33%	-	Copper
Cold	66%	-	Copper
Hot	33%	-	Brass
Cold	33%	345°C, 1.5 h	Copper
Cold	66%	345°C, 1.5 h	Copper with slight cube components
Hot	33%	345°C, 1.5 h	Brass
Cold	33%	510°C, 0.05 h	Copper
Cold	33%	510°C, 0.17 h	Copper w/ abnormal grain growth

CHAPTER 5

INVESTIGATION OF PLC BANDS IN 5754 ALUMINUM ALLOY UNDER VARIOUS STRAIN PATHS

5.1. General Strain Localization Analysis

Since one challenge of the cruciform testing in the literature is the localization of the strain in the center of the sample, it is necessary to check overall strain distribution during testing before analysis about PLC bands. For this purpose, few images taken from stretching under equibiaxial condition was used and strain maps are given in Figure 5.1. The last image belongs just before the fracture point. DIC results show that for both x and y axis, strain is localized at the center with shape of diagonal bands. Maximum strain value is approximately 0.49 where fracture initiates, and minimum strain values are 0.1 at the four edges outside the bands along x direction. On the other hand, for y direction, maximum strain is 0.26 and minimum strain is 0.06. The combination of these values makes the equivalent median strain 0.4 calculated by the DIC software.

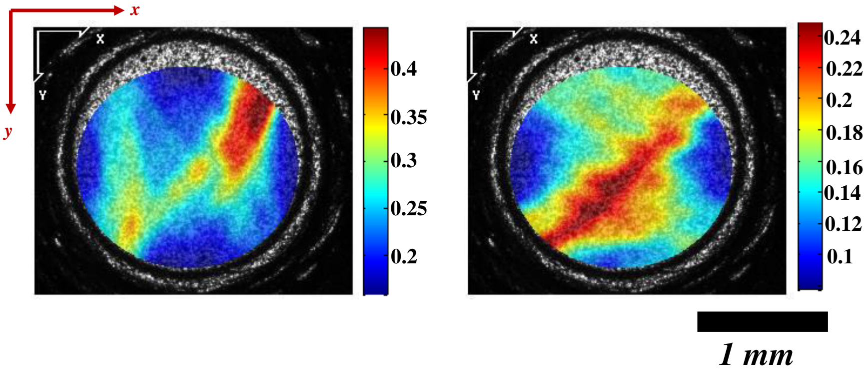

Figure 5.1. Overall DIC result (strain map) of the sample in x direction (left) and in y direction (right) under equibiaxial stretching

For uniaxial loading, unfortunately it is hard to precisely obtain the overall DIC result from image just before the fracture point because of the elongation of the gage region. Therefore, the last image was chosen according to where 2 mm pit region is out of field. While the exact value of the fracture strain cannot be calculated, overall strain localization characteristics can be obtained. Figure 5.2 shows that the localization is in the range of the pit region and observation of PLC bands from the pit region can be accurate.

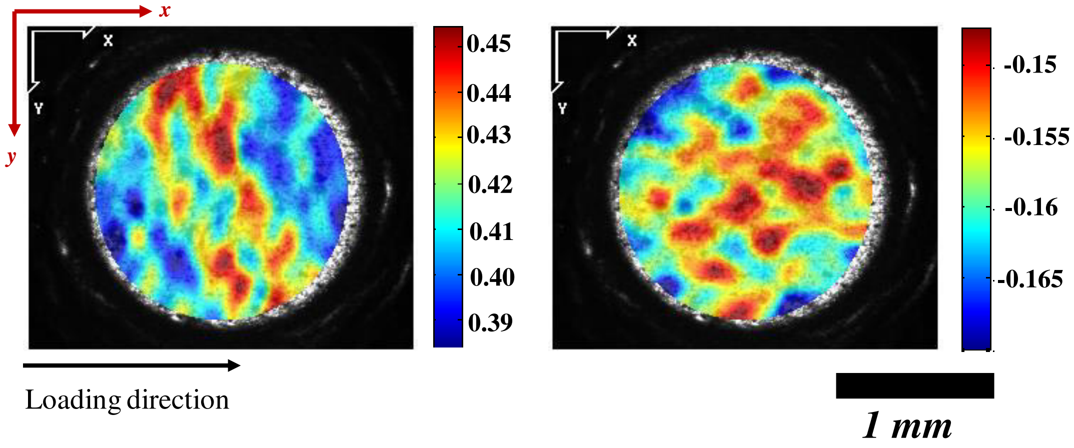

Figure 5.2. Overall DIC result (strain map) of the sample in x direction (left) and in y direction (right) under uniaxial stretching

5.2. Load-Time, Stress-Time & Flow Curves

Figure 5.3 shows differences in load response (in x direction) of the material under uniaxial and biaxial loading with respect to time and strain. Load-time curves in Figure 5.4 were converted to load-strain curves in Figure 5.5 by finding the strain values from DIC analysis at a given time.

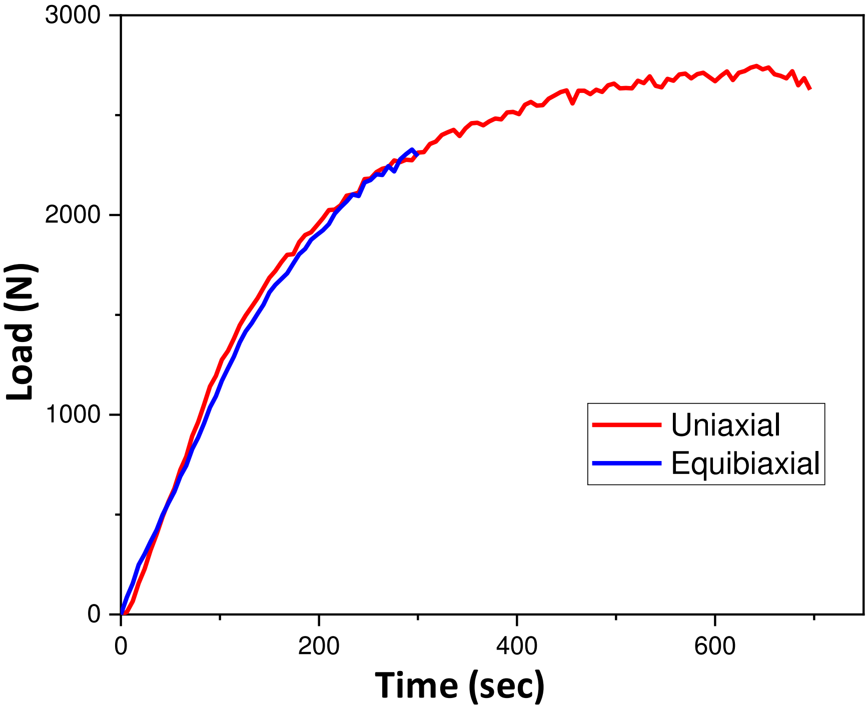

Figure 5.3. Load versus time graph of the material under uniaxial and equibiaxial condition

The load increase behavior is similar for both conditions (Figure 5.3). This figure contains the most representative curves after four tests for each condition. Materials deform with almost same hardening rate, yet the sample under biaxial tension fails at 0.17 engineering strain in x direction and 0.34 equivalent strain (Figure 5.4). After this point, the material under uniaxial stretching continues to deform up to approximately 700 s, corresponding to an engineering and equivalent strain of approximately 0.70 until fracture (Figure 5.4 Material shows no localized neck region and there is no remarkable load drop at fracture under both conditions due to nature of the biaxial testing apparatus and specimen design as explained in elsewhere [81].

While material undergoes additional deformation under uniaxial loading, serrations of the curve due to the PLC effect seem to be more distinct in uniaxial case. Observed serration numbers under uniaxial loading are five times higher than that of under biaxial loading. Average load jump and drop amount is approximately 15 N for biaxial stretching, whereas it is 23 N for uniaxial stretching. Uniaxial condition leads to higher load jumps and drops during deformation. Load jumps and drops are also more remarkable and higher near the end of the test than beginning of the test for uniaxial case. This can be the reason for higher average jump values than equibiaxial case. The first observed PLC band (serration) is seen at earlier stages (at time nearly 180 s) of the testing under uniaxial loading. Furthermore, there are no strict sequence of load jumps and drops with respect to time, indicating that the characteristics of the PLC bands are near to the Type C.

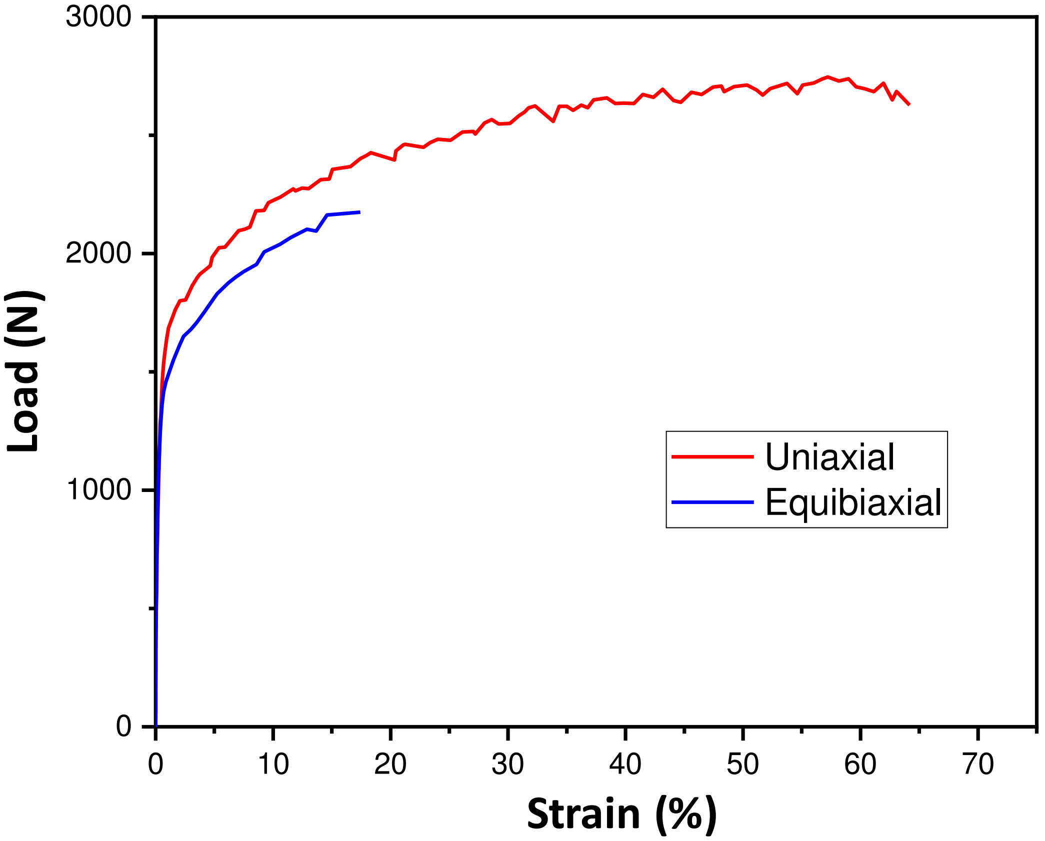

Figure 5.4. Load versus strain graph of the material under uniaxial and equibiaxial condition

Equivalent stress-strain graph (Figure 5.5) of the material also shows that hardening behavior of the material under both conditions are similar. According to calculated strain hardening exponents from plastic region after fitting the curve, it can be stated that the test apparatus does not play role to affect the deformation characteristics of the same material. Moreover, as mentioned above, there is no decrease in the stress value as a result of absence of localized neck region. All in all, forming behavior of the material is independent from formed PLC bands.

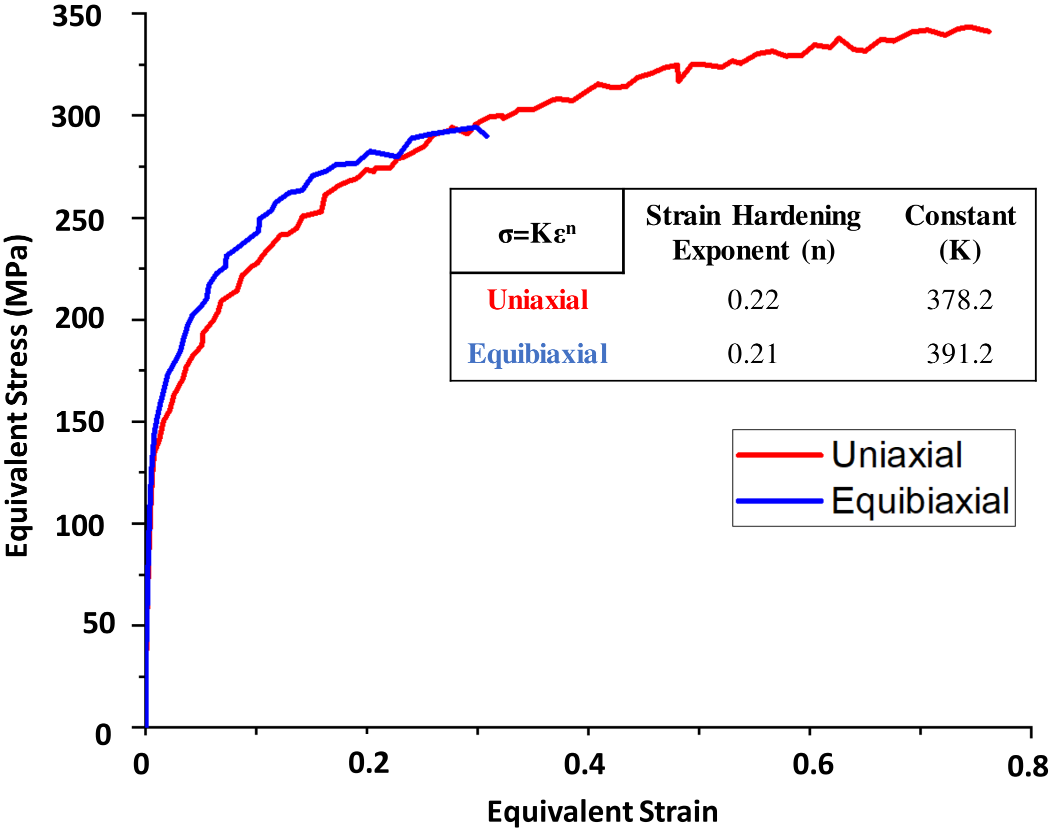

$\sigma=K\varepsilon^n$	Strain Hardening Exponent (n)	Constant (K)
Uniaxial	0.22	378.2
Equibiaxial	0.21	391.2

Figure 5.5. Stress versus strain graph of the material under uniaxial and equibiaxial condition

5.3. Spatial Analysis

2D DIC analysis gives the shape and strain amount in the PLC band by calculating strain distribution of the pit region by taking two consecutive images at each load jump and drop during the test. The DIC results (ε_{xx} direction) in Figure 5.6 were taken from different load jumps and drops during uniaxial tension. Red and yellow regions in the figure show strain localized regions. Shape of the PLC bands is sharp and distinct under uniaxial stretching, it also has an angle of 50° to the loading direction. The blue regions represent nearly strain-free regions and approximately half of the total area is strain-free; therefore, the deformation of the material is heterogeneous, where the strain is localized only in the PLC bands. Strain calculated in the PLC band from beginning to end of the test differs by 0.015 and the maximum strain is 0.026. Load increase during the test is responsible from the strain increase in the formed PLC bands. Also, multiple PLC bands can form at the same time, and these bands can either cross or be parallel to each other. The width of the bands differs from 150 μm to 400 μm. The strain distribution of individual PLC band has higher values through the centerline of the band and the strain usually peaks at one end of the centerline. The PLC bands are also repetitive; they can from at the same region at any time. However, nucleation and propagation of the bands do not have a sequence and they appear to be completely random.

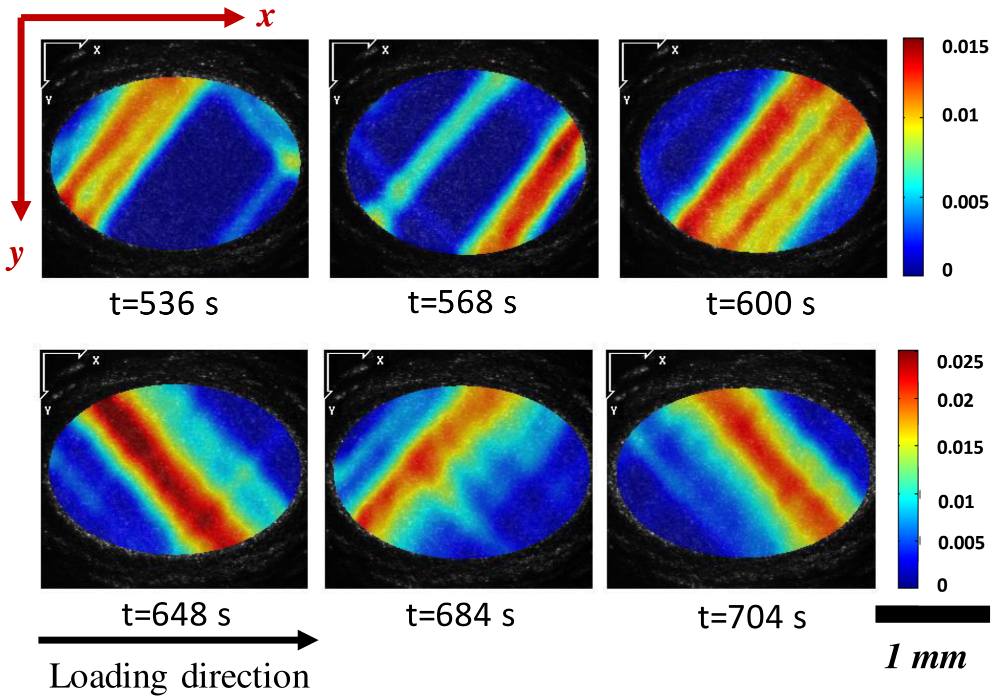

Figure 5.6. Strain distribution maps of the material from different time intervals under uniaxial condition

DIC results in ε_{xx} direction of deformation during biaxial testing of the material (Figure 5.7) show different strain distribution compared to uniaxial testing (Figure 5.6). Instead of sharp, pronounced, and angled bands, there are diffuse and shifted bands formed under biaxial stretching. In this case, the strain-free blue regions cover approximately one third of the gage area. Strain values have a peak at the edge region as in uniaxial condition. However, the strain is not localized along the centerline of the PLC bands. The strain is lower in the middle of the pit region compared to the edge regions. Previous work on the testing apparatus [46] showed that shear strain is negligible at the center region having 1 mm diameter during biaxial stretching. Coincidentally, the continuity of the PLC band is disrupted at the same region where there is no shear strain, indicating that the shear strain is critical in the formation of bands. Towards the end of the test, two PLC bands cross each other, which is visible by “X” shape in the strain maps (Figure 5.7). Maximum detected strain in the formed PLC bands is approximately 0.025 and it is very close to the uniaxial condition. Moreover, the strain localization during biaxial stretching is observed always at the same region. When strain localizations are examined, higher amounts are observed near the edge of gage, where it is twice the strain accumulated at the center.

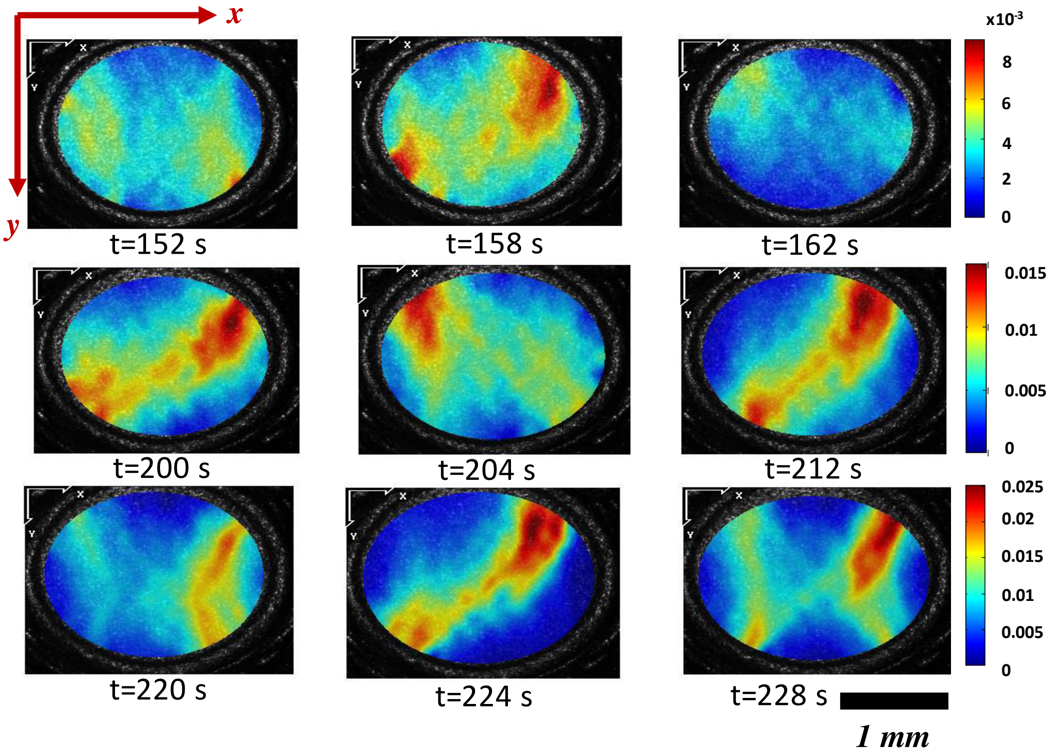

Figure 5.7. Strain distribution maps of the material from different time intervals under equibiaxial condition

5.4. Temporal Analysis

Strain-time plots of the material during testing do not show linear behavior as shown in Figure 5.8. Curves are also serrated due to the strain jumps from PLC bands. Slopes of the curves after elastic deformation are also different and strain-time plot of biaxial testing shows a steeper strain rise with time compared to the uniaxial condition.

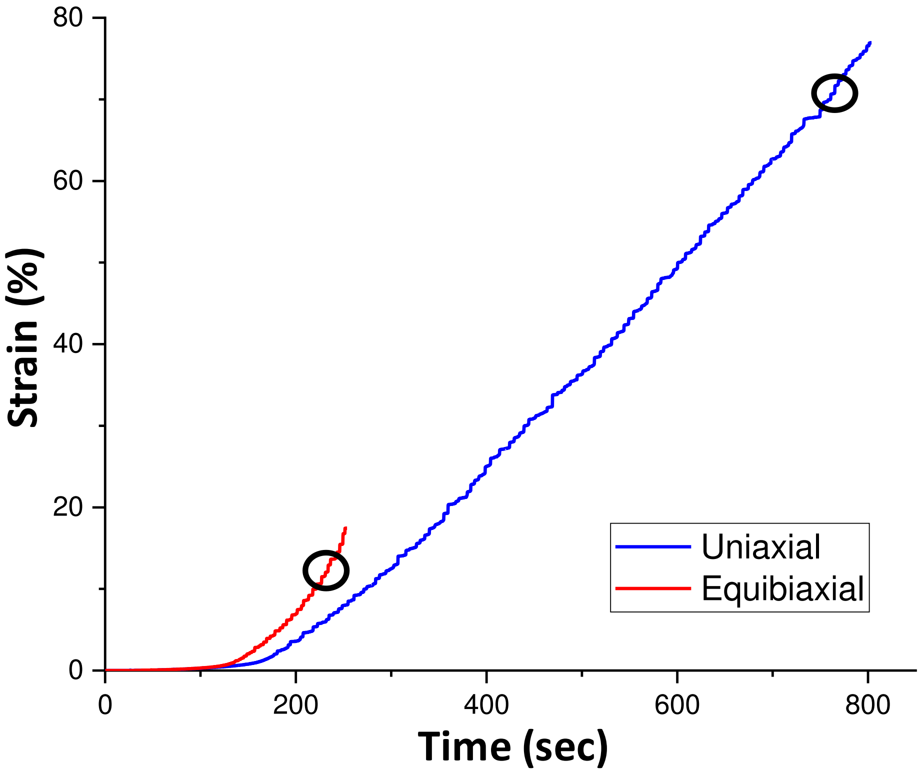

Figure 5.8. Strain versus time graph of the material under uniaxial and equibiaxial condition

Figure 5.9a and 5.9b give the strain changes from each PLC band clearly. For a given time interval, the number of strain jumps under uniaxial loading is higher than the biaxial condition, highlighting the importance of strain path for PLC formation. Under shear dominated stress state (uniaxial stretching), PLC effects seem to be clearer. Average strain jump under uniaxial stretching is 0.0055 while it is 0.0059 under biaxial stretching. Towards the end of the test, PLC bands cross each other in biaxial condition, resulting in higher strain jumps than usual. The strain increase between two successive bands is only 0.001 under both uniaxial and biaxial conditions.

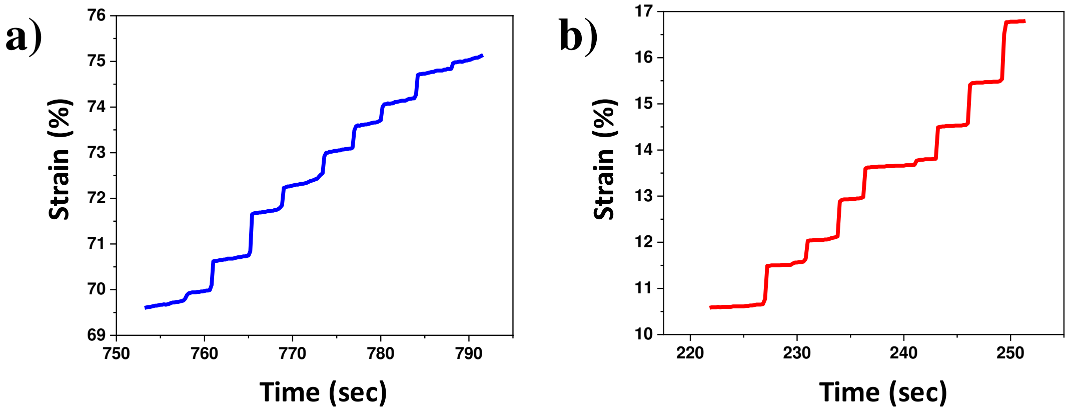

Figure 5.9. Zoomed view of strain versus time curves of a) uniaxial b) equibiaxial condition indicated with circles in Figure 5.8

The strain contribution of PLC bands to overall deformation is given in Figure 5.10. This figure was created by summing each obvious strain jump from Figure 5.8 and dividing them to the overall strain calculated by DIC software during deformation. The contribution of all strain jumps to the overall deformation in biaxial and uniaxial condition are 84% and 75%, respectively. Since the negative effects of the PLC bands in the deformation, such as negative strain rate sensitivity, lower formability and poor surface finish are known; the higher PLC contribution in biaxial stretching is expected to affect the material more negatively. The other interesting point is that contribution of PLC band strain is linear with respect to overall strain. This linearity is higher in equibiaxial condition than uniaxial condition. It can be the other reason for expectation of negative effects. However, the load-time and load-strain graphs showed that the formability was unaffected with the strain path change (Figure 5.3, 5.4 and 5.5). Under both conditions, material deformed until typical fracture strains. Therefore, even the majority of strain is localized to the PLC bands under both conditions; the overall formability does not depend on them significantly.

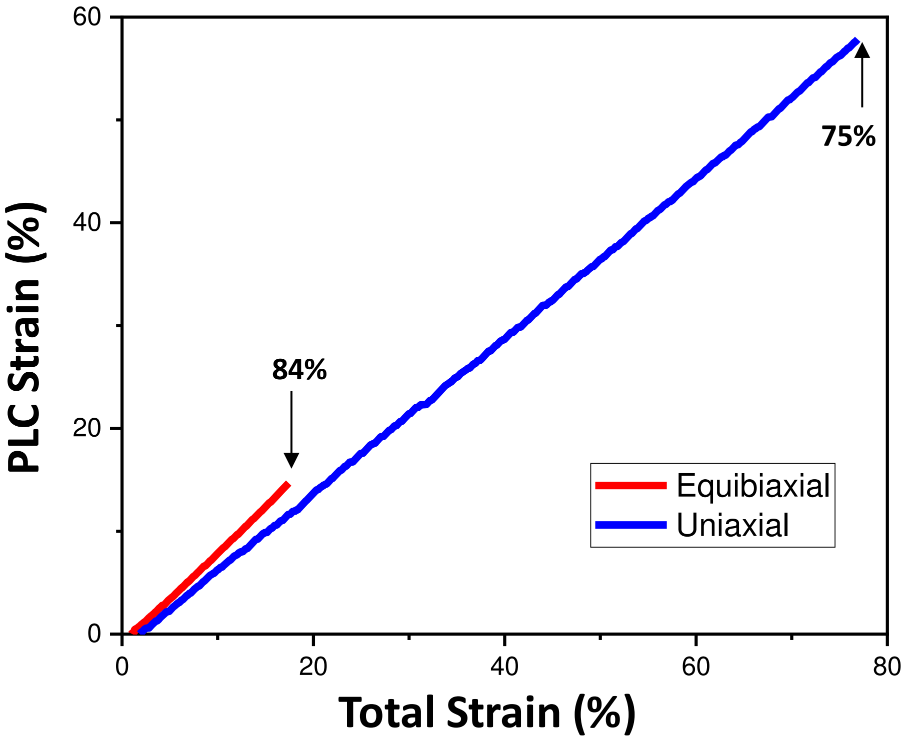

Figure 5.10. Strain contribution of PLC bands versus total strain graph under uniaxial and biaxial condition (along xx direction)

5.5. Shear Band Analysis & Surface Examination

Besides the strain heterogeneity, a more significant drawback of the PLC bands is the formation of shear bands. Under uniaxial tension, the repetitive formation of PLC bands in a particular region of the sample leads to a shear band at the same region. Figure 5.11 shows the formation of one of the shear band during uniaxial stretching. The first visible shear band (showed with white dashed lines) during testing exists at time t=9 minutes. These photographs are sequential at stated time intervals. At time t_1, t_2 and t_3; repeated PLC bands create a nucleation site for the shear band. For t_3=12 min, shear band is seen more clearly. However, showing these PLC bands is hard with the taken images from digital camera because of the contrast. After nucleation, PLC band strain is contributed to the nucleated shear band during loading. All in all, this causes to formation of visible shear band and widening of this band.

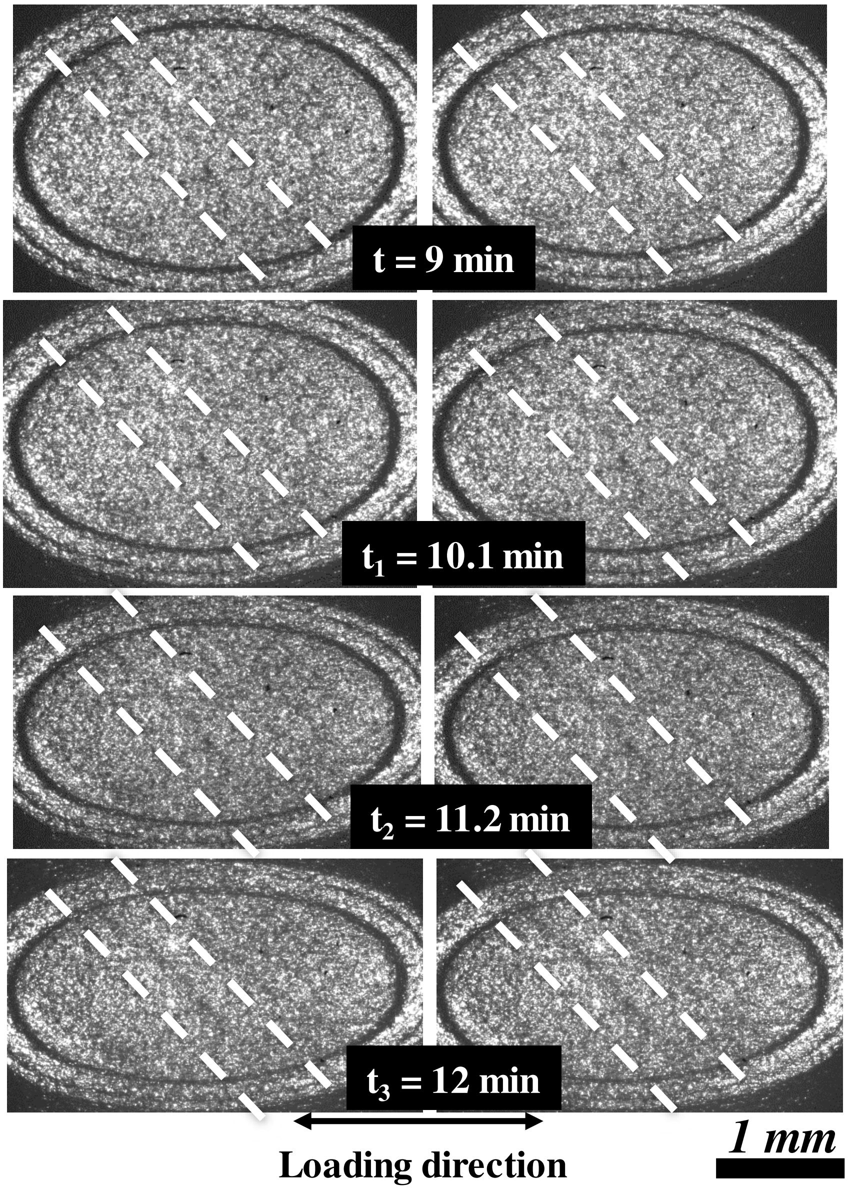

Figure 5.11. Steps of formation of shear band due to PLC bands at time between 9 minutes and 13 minutes during uniaxial tension (White dashed lines show the repeated PLC bands and formed shear band.)

PLC bands create nucleation sites for the shear bands and this is also observed by Kang et al. [82] and Yoshida et al. [83]. Shear stress state in uniaxial case promotes full-scale PLC bands that stretch through the whole gage length, whereas in biaxial they form only to a limited extent because global shear stresses are zero (Figure 5.7).

The local resolved shear stresses cause slip and therefore PLC bands in biaxial case, however they do not grow fully. In uniaxial case, on the other hand, a collection of full-scale PLC bands in the same region of the sample avalanche into a shear band, where further shear strains accumulate (Figure 5.12). This figure obtained from the surface of the specimen after deformation. Prior to deformation, the specimen pit region was electropolished. Single shear band in uniaxial contains multiple PLC bands that appear as surface irregularities in Figure 5.12. The shear bands then cross each other, which also causes catastrophic failure from the same regions. Conversely, there are no surface irregularities or shear bands observed on the surface after biaxial deformation.

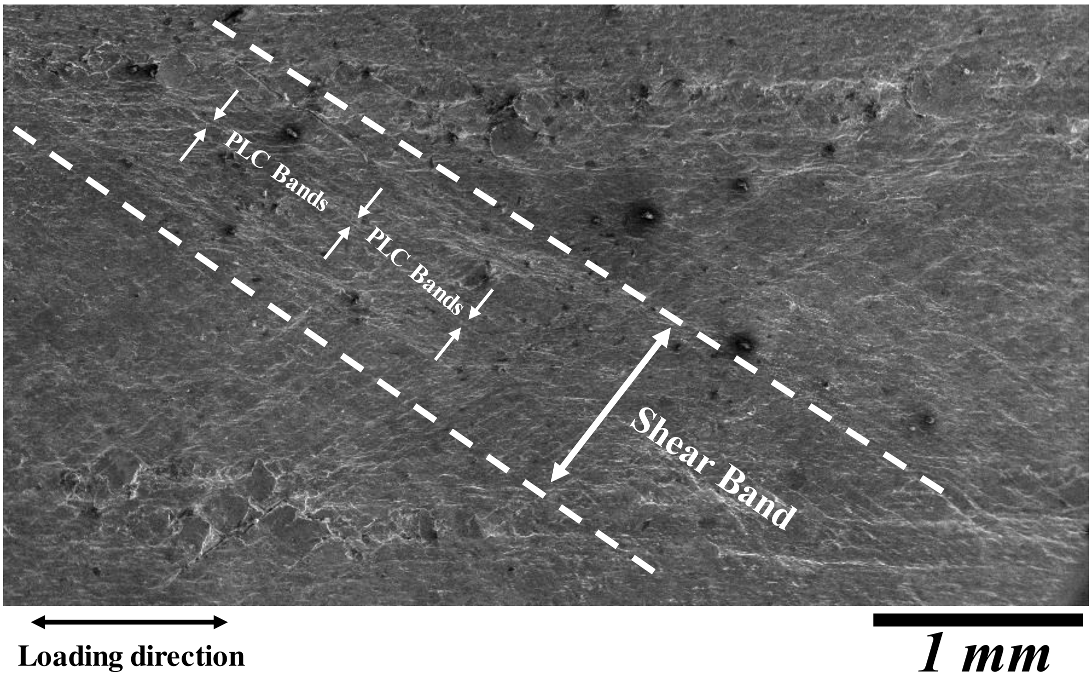

Figure 5.12. SEM image of formed shear bands after uniaxial tension

Close view of the shear band of Figure 5.13 shows that PLC bands cause surges on the deformed surface. Formation of slip bands by PLC bands and crossing action of these bands result in the small cracks and spreading between grains such as triple junctions. All in all, these are the initiation sites of the catastrophic failure in micron scale.

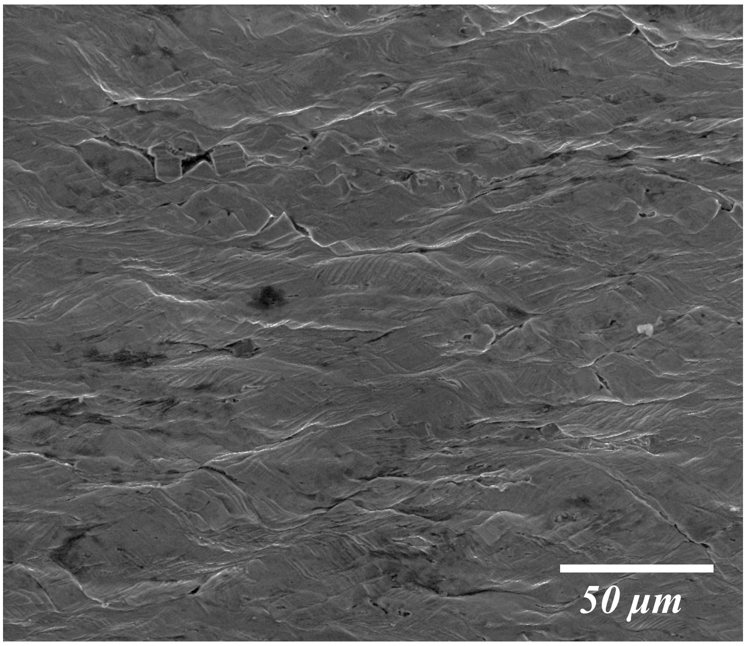

Figure 5.13. SEM image of zoomed view of shear band showing surface irregularities

5.6. Fracture Analysis

Figure 5.14 shows the images of the pit region after both uniaxial and equibiaxial condition. In biaxial condition (Figure 5.14a), expansion of the pit region is homogenous due to equal forces along x and y direction. Fracture occurred with an angle of 45°. It can be stated that crack initiates and propagates along dominant cross line of X shaped PLC band without forming any shear band. For uniaxial condition (Figure 5.14b), excess elongation in loading direction is obvious and fracture occurred along one of the formed shear bands. The second shear band nearly perpendicular to other is also seen in Figure 5.14b (showed with red arrow). Crack was initiated and propagated along one of the shear band.

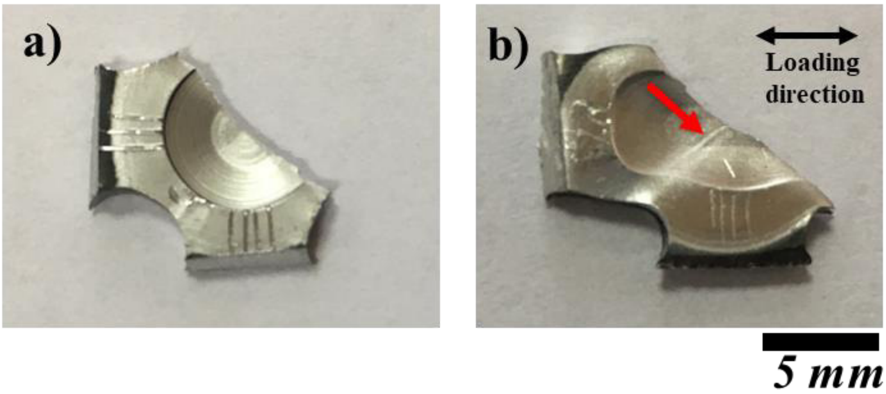

Figure 5.14. Images of gage region of the specimen after a) equibiaxial condition b) uniaxial condition

Region around fracture under uniaxial stretching is shown in Figure 5.15a. Clustering of surface irregularities resulting from PLC bands is clearly seen and shown with white arrows. Fracture also occurred from shear bands. Fracture surfaces shown in Figure 5.15b prove that the fracture and deformation mode of the uniaxial tension is shear-based and relatively brittle. Shear bands formed (red arrow in Figure 5.15b) due to the PLC bands result in elongated sharp dimples.

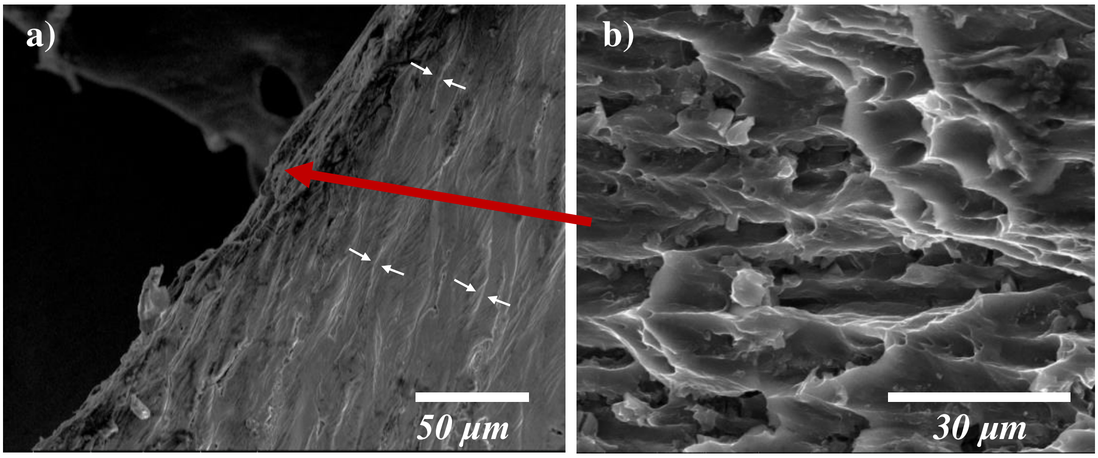

Figure 5.15. SEM images of a) region around fracture b) fracture surface after uniaxial stretching (Red arrow shows the top view of the marked region.)

Deformed surface of the material after equibiaxial stretching is given in Figure 5.16a. The region around fracture has no clustering of PLC bands. The fracture surface after biaxial stretching has a typical ductile fracture structure with round dimples (Figure 5.16b).

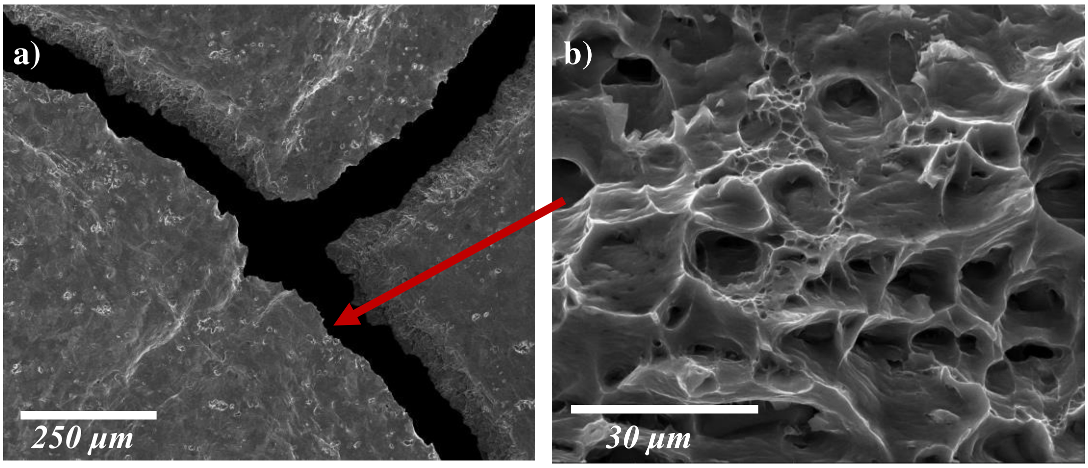

Figure 5.16. SEM images of a) region around fracture b) fracture surface after biaxial stretching (Red arrow shows the top view of the marked region.)

5.7. Texture Evolution

EBSD analysis shows the deformation microstructures and textures for both strain paths at a constant equivalent strain, $\varepsilon_{eq} = 0.18$. In biaxial stretching, deformation texture is brass (Figure 5.17a and 5.17b), parallel to the observations in literature [51]. The brass texture is not far off from the initial copper texture.

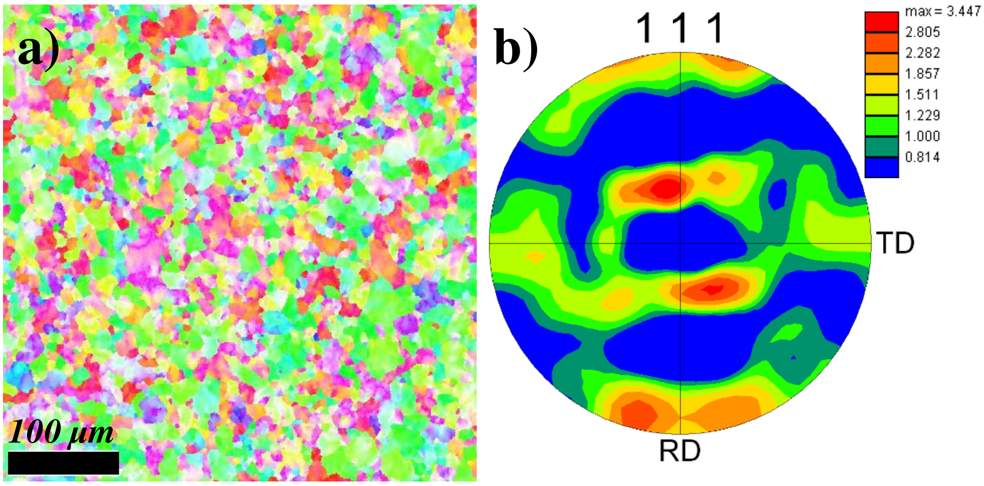

Figure 5.17. EBSD analysis of the specimen a) grain orientation map b) 111 pole figure after equibiaxial loading

In uniaxial condition, on the other hand, an increase in cube component of the texture is obvious. The initial copper texture evolves into a cube texture after sufficient deformation as shown in Figure 5.18a and 5.18b. Therefore, it is once again proved that the shear bands dominate the deformation in uniaxial condition. Since the cube texture component is a result of shear-based deformation in aluminum alloys, the increase in this texture component explains the relationship between PLC and shear bands. The texture change in the material is not due to a single PLC band, but rather a collection of them, which evolve into the shear bands. The combination of the shear bands with the strain path is responsible from the significant change in texture.

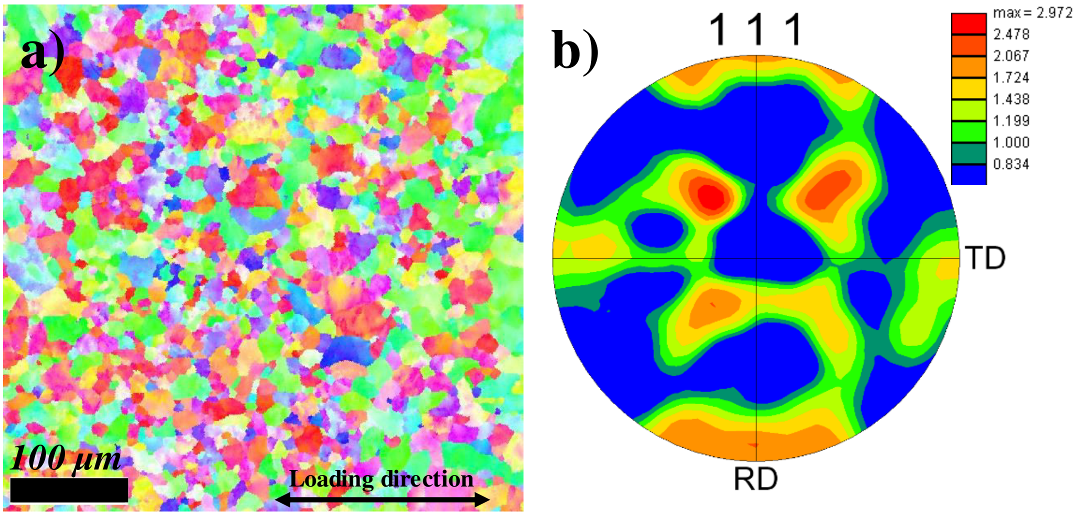

Figure 5.18. EBSD analysis of the specimen a) grain orientation map b) 111 pole figure uniaxial loading

The cube component of the uniaxial condition is clearer when the EBSD analysis was done on the formed shear band shown in Figure 5.19. The EBSD result from the shear band contains many black spots, where the diffraction quality was poor. This is due to the high deformation amounts ($\varepsilon > 0.3$) within the band, which limits the quality of the data. However, the remaining data is enough to confirm that the {001}<100> texture component is activated in uniaxial loading due to the shear bands. Lack of full-scale PLC bands and the shear bands in biaxial stretching prevents this kind of texture change and keeps the initial texture with minor changes.

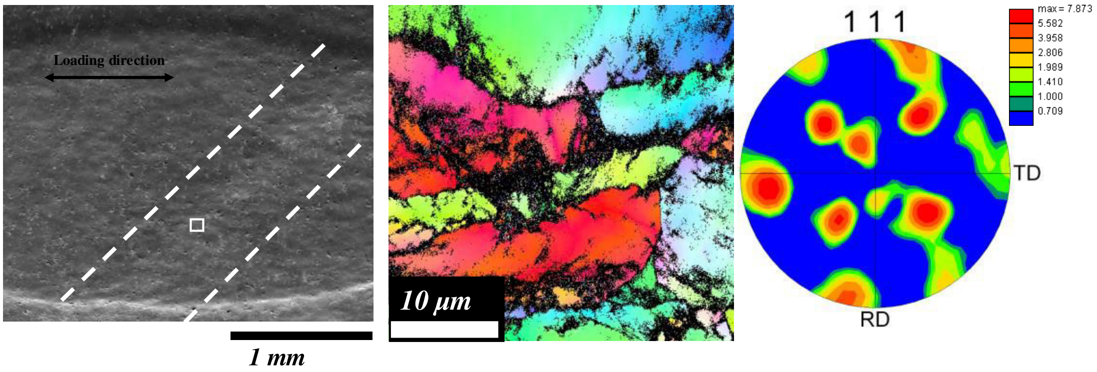

Figure 5.19. EBSD result of the first formed shear band

CHAPTER 6

CONCLUSIONS & FUTURE WORKS

In this thesis; first of all, rolling operation was applied to the 5754 aluminum alloy under both hot (33% reduction in thickness at 480°C) and cold (33% and 66% reduction in thickness at room temperature) condition. Resulting microstructure and texture were investigated by EBSD analysis. Both rolled and annealed (345°C for 1.5 h) states were analyzed. After deformation and recrystallization following conclusions can be reached:

- Cold rolling with small reduction in thickness (33%) results in typical copper type texture. Annealing operation does not change the texture components. However, it changes the microstructure with recrystallization phenomena.
- Cold rolling with high reduction in thickness (66%) does not change the initial texture of material (copper type texture). However, annealing increases the nucleation sites of grains having cube textures.
- Hot rolling results in brass texture which is slightly deviated from copper texture and annealing has no effect on the texture.
- High annealing temperatures and relatively higher annealing times (510°C and 10 minutes, respectively) causes dissolution of second phase particles and abnormal grain growth of some specified grains. Grains having different orientation from {111} tend to grow abnormally.

In the second part of this thesis, PLC bands were investigated under different loading conditions (equibiaxial and uniaxial). After spatio-temporal analysis of PLC bands, SEM analysis of deformed surfaces and fracture surfaces, and EBSD analysis of deformed specimen, following remarks are the main results of this thesis:

- Load jumps is higher in the uniaxial condition towards the end of the test. However, strain hardening exponent calculations shows that forming characteristics of the alloy is not affected from the strain paths.
- Spatial analysis show that while PLC bands are sharp and have 50° to the loading axis in uniaxial condition, it is diffuse and nearly cross (X) shaped in equibiaxial condition.
- Temporal analysis of strain shows that the amount of PLC bands is higher in uniaxial condition. However, crossed action of PLC bands in equibiaxial condition makes strain jumps higher compared to uniaxial condition.
- While total strain coming from PLC bands is higher under equibiaxial condition, surface irregularity amount is higher under uniaxial condition. Surface irregularities show themselves as shear bands and shear bands extremely disrupt the surface quality, so they cause catastrophic failure.
- There are two different fracture surfaces for this study. One of them has round typical dimples after equibiaxial loading, other one has elongated dimples after uniaxial loading.
- During uniaxial and equibiaxial loading, the texture of material varies differently. For equibiaxial condition, final product has brass type texture. For uniaxial condition, cube components in the pole figure is obvious because of acting shear forces.

Recommended future works for this thesis are as follows:

- Spatio-temporal analysis under plane strain condition or other strain paths can be done with same DIC and test setup.
- The texture of initial material can be changed with rolling experiments and PLC bands and their effects to different textures from copper texture can be analyzed.
- Micro-scale (grain-scale) investigation of the PLC bands in terms of spatial analysis can be done with same experimental setup.

- Deformation processes including rolling can be optimized to suppress PLC bands by eliminating the acting shear forces.

REFERENCES

[1] ASM International, “Aluminum Properties and Physical Metallurgy,” J. E. Hatch, Ed. 1984, pp. 48–49.

[2] J. G. Kaufman, “Understanding the Aluminum Temper,” in *Introduction to Aluminum Alloys and Tempers*, 2000, pp. 39–76.

[3] F. J. Humphreys and M. Hatherly, “Deformation Textures,” in *Recrystallization and Related Annealing Phenomena*, 2004, pp. 67–89.

[4] H. Weiland and J. R. Hirsch, “Microstructure and Local Texture in Hot Rolled Aluminum,” *Textures Microstruct.*, vol. 14, no. C, pp. 647–652, 1991.

[5] A.H. Cottrell, “Theory of dislocations,” *Prog. Met. Phys.*, vol. 4, pp. 249–264, 1953.

[6] R. W. Hertzberg, R. P. Vinci, and J. L. Hertzberg, *Deformation and Fracture Mechanics of Engineering Materials*. John Wiley & Sons, 2013.

[7] P. G. McCormick, “The Portevin-Le Chatelier effect in an Al-Mg-Si alloy,” *Acta Metall.*, vol. 19, no. 5, pp. 463–471, 1971.

[8] R. A. Mulford and U. F. Kocks, “New observations on the mechanisms of dynamic strain aging and of jerky flow,” *Acta Metall.*, vol. 27, no. 7, pp. 1125–1134, 1979.

[9] A. W. Sleeswyk, “Slow strain-hardening of ingot iron,” *Acta Metall.*, vol. 6, no. 9, pp. 598–603, 1958.

[10] A. A. Shibkov, M. A. Zheltov, M. F. Gasanov, and A. E. Zolotov, “Dynamics of a Lüders Band and Destruction of an Aluminum-Magnesium Alloy, Initiated by a Stress Concentrator,” *Phys. Solid State*, vol. 60, no. 2, pp. 320–327, 2018.

[11] A. Yilmaz, “The Portevin-Le Chatelier effect: A review of experimental

findings," *Sci. Technol. Adv. Mater.*, vol. 12, no. 6, pp. 1–17, 2011.

[12] A. Beaudoin *et al.*, "On the sequence of inhomogeneous deformation processes occurring during tensile deformation of strip cast AA5754," *Acta Mater.*, vol. 54, no. 1, pp. 209–218, 2005.

[13] A. V. Shuklinov, A. A. Denisov, M. A. Zheltov, A. E. Zolotov, and A. A. Shibkov, "Dynamics of deformation bands and fracture of the aluminum-magnesium alloy 5556," *Phys. Solid State*, vol. 53, no. 10, pp. 1975–1980, 2011.

[14] D. Yuzbekova, A. Mogucheva, D. Zhemchuzhnikova, T. Lebedkina, M. Lebyodkin, and R. Kaibyshev, "Effect of microstructure on continuous propagation of the Portevin-Le Chatelier deformation bands," *Int. J. Plast.*, vol. 96, pp. 210–226, 2017.

[15] J. Hirsch and T. Al-Samman, "Superior light metals by texture engineering: Optimized aluminum and magnesium alloys for automotive applications," *Acta Mater.*, vol. 61, no. 3, pp. 818–843, 2013.

[16] S. D. Antolovich and R. W. Armstrong, "Plastic strain localization in metals: Origins and consequences," *Prog. Mater. Sci.*, vol. 59, no. 1, pp. 1–160, 2014.

[17] H. Jiang *et al.*, "Three types of Portevin-Le Chatelier effects: Experiment and modelling," *Acta Mater.*, vol. 55, no. 7, pp. 2219–2228, 2007.

[18] A. Chatterjee, K. L. Murty, N. Gayathri, P. Mukherjee, and P. Barat, "Temperature dependence of the dynamics of Portevin-Le Chatelier effect in Al-2.5 Pct Mg Alloy," *Metall. Mater. Trans. A Phys. Metall. Mater. Sci.*, vol. 42, no. 5, pp. 1184–1190, 2011.

[19] H. Ait-Amokhtar and C. Fressengeas, "Crossover from continuous to discontinuous propagation in the Portevin-Le Chatelier effect," *Acta Mater.*, vol. 58, no. 4, pp. 1342–1349, 2010.

[20] W. Wen, Y. Zhao, and J. G. Morris, “The effect of Mg precipitation on the mechanical properties of 5xxx aluminum alloys,” *Mater. Sci. Eng. A*, vol. 392, no. 1–2, pp. 136–144, 2005.

[21] N. Tian, G. Wang, Y. Zhou, K. Liu, G. Zhao, and L. Zuo, “Study of the Portevin-Le Chatelier (PLC) characteristics of a 5083 aluminum alloy sheet in two heat treatment states,” *Materials (Basel).*, vol. 11, no. 9, pp. 1–16, 2018.

[22] A. H. Clausen, T. Børvik, O. S. Hopperstad, and A. Benallal, “Flow and fracture characteristics of aluminium alloy AA5083-H116 as function of strain rate, temperature and triaxiality,” *Mater. Sci. Eng. A*, vol. 364, no. 1–2, pp. 260–272, 2004.

[23] H. Jiang, Q. Zhang, X. Wu, and J. Fan, “Spatiotemporal aspects of the Portevin-Le Chatelier effect in annealed and solution-treated aluminum alloys,” *Scr. Mater.*, vol. 54, no. 12, pp. 2041–2045, 2006.

[24] G. Saad, S. A. Fayek, A. Fawzy, H. N. Soliman, and E. Nassr, “Serrated flow and work hardening characteristics of Al-5356 alloy,” *J. Alloys Compd.*, vol. 502, no. 1, pp. 139–146, 2010.

[25] J. Min, L. G. Hector, J. E. Carsley, T. B. Stoughton, B. E. Carlson, and J. Lin, “Spatio-temporal characteristics of plastic instability in AA5182-O during biaxial deformation,” *Mater. Des.*, vol. 83, pp. 786–794, 2015.

[26] H. Hamasaki and F. Tamashiro, “Biaxial deformation on AA5182-O aluminium alloy sheet at warm temperature,” in *Journal of Physics: Conference Series*, 2018, vol. 1063, no. 1, pp. 1–5.

[27] M. A. Iadicola, L. Hu, A. D. Rollett, and T. Foecke, “5754 aluminum sheet deformed along Bi-linear strain paths,” *AIP Conf. Proc.*, vol. 1383, no. 2011, pp. 299–306, 2011.

[28] J. B. Le Cam, E. Robin, L. Leotoing, and D. Guines, “Calorimetric analysis of Portevin-Le Chatelier bands under equibiaxial loading conditions in Al–Mg

alloys: Kinematics and mechanical dissipation," *Mech. Mater.*, vol. 105, pp. 80–88, 2017.

[29] X. Song, L. Leotoing, D. Guines, and E. Ragneau, "Investigation of the forming limit strains at fracture of AA5086 sheets using an in-plane biaxial tensile test," *Eng. Fract. Mech.*, vol. 163, pp. 130–140, 2016.

[30] Y. Hou, J. Min, J. Lin, J. E. Carsley, and T. B. Stoughton, "Plastic instabilities in AA5754-O under various stress states," *IOP Conf. Ser. Mater. Sci. Eng.*, vol. 418, no. 1, pp. 1–8, 2018.

[31] G. T. Motsi, P. A. Olubambi, T. J. Sono, and L. Shoke, "*In Situ* Electron Microscopy Studies on the Tensile Deformation Mechanisms in Aluminium 5083 Alloy," *Adv. Mater. Res.*, vol. 1019, pp. 103–111, 2014.

[32] D. Zhemchuzhnikova, M. Lebyodkin, D. Yuzbekova, T. Lebedkina, A. Mogucheva, and R. Kaibyshev, "Interrelation between the portevin le-chatelier effect and necking in almg alloys," *Int. J. Plast.*, vol. 110, no. June, pp. 95–109, 2018.

[33] Y. Cai, Q. Zhang, S. Yang, S. Fu, and Y. Wang, "Experimental Study on Three-Dimensional Deformation Field of Portevin–Le Chatelier Effect Using Digital Image Correlation," *Exp. Mech.*, vol. 56, no. 7, pp. 1243–1255, 2016.

[34] N. A. Sene, P. Balland, and K. Bouabdallah, "Experimental study of Portevin–Le Châtelier bands on tensile and plane strain tensile tests," *Arch. Civ. Mech. Eng.*, vol. 18, no. 1, pp. 94–102, 2018.

[35] G. E. Totten and D. S. MacKenzie, Eds., "Handbook of Aluminum," in *Marcel Dekker*, vol. 1, 2003, pp. 81–385.

[36] ASM International, "Properties and Selection: Nonferrous Alloys and Special-Purpose Materials," in *ASM International*, vol. 2, 2012, pp. 222–484.

[37] A. K. Vasudevan and R. D. Doherty, Eds., *Aluminum Alloys — Contemporary*

Research and Applications. Academic Press, 1989.

[38] J. L. Murray, "The Al-Mg (Aluminum-Magnesium) system," *Bull. Alloy Phase Diagrams*, vol. 3, pp. 60–73, 1982.

[39] "Aluminium Alloy - Commercial Alloy - 5754 - H22 Sheet and Plate," 2015. [Online]. Available: http://www.aalco.co.uk/datasheets/Aluminium-Alloy-5754-H22-Sheet-and-Plate_153.ashx.

[40] R. E. Sanders, P. A. Hollinshead, and E. A. Simielli, "Industrial development of non-heat treatable aluminum alloys," *Mater. Forum*, vol. 28, pp. 53–64, 2004.

[41] ASM International, "Forming and Forging," in *ASM Metals Handbook*, vol. 14, 2012, pp. 37–39.

[42] F. J. Humphreys and M. Hatherly, "Control of Recrystallization," in *Recrystallization and Related Annealing Phenomena*, 2004, pp. 469–505.

[43] H. Hu, "Texture of Metals," *Texture*, vol. 1, no. 4, pp. 233–258, 1974.

[44] L. A. I. Kestens and H. Pirgazi, "Texture formation in metal alloys with cubic crystal structures," *Mater. Sci. Technol. (United Kingdom)*, vol. 32, no. 13, pp. 1303–1315, 2016.

[45] T. Leffers and D. J. Jensen, "The Relation Between Texture and Microstructure in Rolled FCC Materials," *Textures Microstruct.*, vol. 14, no. C, pp. 933–952, 1991.

[46] J. Hirsch, "Recent development in aluminium for automotive applications," *Trans. Nonferrous Met. Soc. China (English Ed.*, vol. 24, no. 7, pp. 1995–2002, 2014.

[47] J. Hirsch, "Aluminium alloys for automotive application," *Mater. Sci. Forum*, vol. 242, no. January 1997, pp. 33–50, 1997.

[48] O. Engler and J. Hirsch, “Recrystallization textures and plastic anisotropy in Al-Mg-Si sheet alloys,” *Mater. Sci. Forum*, vol. 217–222, pp. 479–486, 1996.

[49] M. H. Alvi, S. W. Cheong, J. P. Suni, H. Weiland, and A. D. Rollett, “Cube texture in hot-rolled aluminum alloy 1050 (AA1050)-nucleation and growth behavior,” *Acta Mater.*, vol. 56, no. 13, pp. 3098–3108, 2008.

[50] S. W. Banovic, M. A. Iadicola, and T. Foecke, “Textural development of AA 5754 sheet deformed under in-plane biaxial tension,” *Metall. Mater. Trans. A Phys. Metall. Mater. Sci.*, vol. 39, no. 9, pp. 2246–2258, 2008.

[51] S. W. Banovic and T. Foecke, “Evolution of strain-induced microstructure and texture in commercial aluminum sheet under balanced biaxial stretching,” *Metall. Mater. Trans. A Phys. Metall. Mater. Sci.*, vol. 34 A, no. 3, pp. 657–671, 2003.

[52] J. R. Donoso and R. E. Reed-Hill, “Static strain-aging in commercial purity alpha titanium,” *Metall. Trans. A*, vol. 8, no. 6, pp. 945–948, 1977.

[53] A. H. Cottrell and B. A. Bilby, “Dislocation Theory of Yielding and Strain Ageing of Iron,” in *Proceedings of the Physical Society*, 1949, pp. 49–62.

[54] A. Benallal, T. Berstad, T. Børvik, O. S. Hopperstad, I. Koutiri, and R. N. de Codes, “An experimental and numerical investigation of the behaviour of AA5083 aluminium alloy in presence of the Portevin-Le Chatelier effect,” *Int. J. Plast.*, vol. 24, no. 10, pp. 1916–1945, 2008.

[55] M. Abbadi, P. Hähner, and A. Zeghloul, “On the characteristics of Portevin - Le Chatelier bands in aluminum alloy 5182 under stress-controlled and strain-controlled tensile testing,” *Mater. Sci. Eng. A*, vol. 337, no. 1–2, pp. 194–201, 2002.

[56] M. Gerland, J. Mendez, J. Lépinoux, and P. Violan, “Dislocation structure and corduroy contrast in a 316L alloy fatigued at (0.3-0.5) Tm,” *Mater. Sci. Eng. A*, vol. 164, no. 1–2, pp. 226–229, 1993.

[57] J. Kang, D. S. Wilkinson, J. D. Embury, M. Jain, and A. J. Beaudoin, “Effect of type-B Portevin-Le Chatelier bands on the onset of necking in uniaxial tension of strip cast AA5754 sheets,” *Scr. Mater.*, vol. 53, no. 5, pp. 499–503, 2005.

[58] K. Chihab, Y. Estrin, L. P. Kubin, and J. Vergnol, “The kinetics of the Portevin-Le Chatelier bands in an Al-5at%Mg alloy,” *Scr. Metall.*, vol. 21, pp. 203–208, 1987.

[59] L. Casarotto, R. Tutsch, R. Ritter, H. Dierke, F. Klose, and H. Neuhäuser, “Investigation of PLC bands with optical techniques,” *Comput. Mater. Sci.*, vol. 32, no. 3–4, pp. 316–322, 2005.

[60] H. Louche, P. Vacher, and R. Arrieux, “Thermal observations associated with the Portevin-Le Châtelier effect in an Al-Mg alloy,” *Mater. Sci. Eng. A*, vol. 404, no. 1–2, pp. 188–196, 2005.

[61] D. Delpueyo, X. Balandraud, and M. Grédiac, “Calorimetric signature of the Portevin-Le Châtelier effect in an aluminum alloy from infrared thermography measurements and heat source reconstruction,” *Mater. Sci. Eng. A*, vol. 651, pp. 135–145, 2016.

[62] B. Pan, K. Qian, H. Xie, and A. Asundi, “Two-dimensional digital image correlation for in-plane displacement and strain measurement: A review,” *Meas. Sci. Technol.*, vol. 20, no. 6, pp. 1–17, 2009.

[63] H. Halim, D. S. Wilkinson, and M. Niewczas, “The Portevin-Le Chatelier (PLC) effect and shear band formation in an AA5754 alloy,” *Acta Mater.*, vol. 55, no. 12, pp. 4151–4160, 2007.

[64] Y. Cai, S. Yang, S. Fu, D. Zhang, and Q. Zhang, “Investigation of Portevin–Le Chatelier Band Strain and Elastic Shrinkage in Al-Based Alloys Associated with Mg Contents,” *J. Mater. Sci. Technol.*, vol. 33, no. 6, pp. 580–586, 2017.

[65] Y. L. Cai, S. L. Yang, Y. H. Wang, S. H. Fu, and Q. C. Zhang, “Characterization

of the deformation behaviors associated with the serrated flow of a 5456 Al-based alloy using two orthogonal digital image correlation systems," *Mater. Sci. Eng. A*, vol. 664, pp. 155–164, 2016.

[66] T. Makkinen, "Portevin – Le Chatelier effect in an aluminum alloy," Aalto University, 2016.

[67] R. Shabadi, S. Kumar, H. J. Roven, and E. S. Dwarakadasa, "Effect of specimen condition, orientation and alloy composition on PLC band parameters," *Mater. Sci. Eng. A*, vol. 382, no. 1–2, pp. 203–208, 2004.

[68] W. Wen and J. G. Morris, "An investigation of serrated yielding in 5000 series aluminum alloys," *Mater. Sci. Eng. A*, vol. 354, no. 1–2, pp. 279–285, 2003.

[69] P. cheng Ma, D. Zhang, L. zhong Zhuang, and J. shan Zhang, "Effect of alloying elements and processing parameters on the Portevin-Le Chatelier effect of Al-Mg alloys," *Int. J. Miner. Metall. Mater.*, vol. 22, no. 2, pp. 175–183, 2015.

[70] A. Sarkar, P. Barat, and P. Mukherjee, "Investigation of portevin-le chatelier effect in Al-2.5 pct Mg alloy with different microstructure," *Metall. Mater. Trans. A Phys. Metall. Mater. Sci.*, vol. 44, no. 6, pp. 2604–2612, 2013.

[71] W. Wen and J. G. Morris, "The effect of cold rolling and annealing on the serrated yielding phenomenon of AA5182 aluminum alloy," *Mater. Sci. Eng. A*, vol. 373, no. 1–2, pp. 204–216, 2004.

[72] A. Astarita, M. Liberini, C. Velotti, C. Sinagra, and A. Squillace, "Experimental study of the Portevin-Le Chatelier effect in AA 5754 sheets: Influence of the different rolling routes," in *AIP Conference Proceedings*, 2016, vol. 1769, pp. 130007-1–6.

[73] D. A. Zhemchuzhnikova, M. A. Lebyodkin, T. A. Lebedkina, and R. O. Kaibyshev, "Unusual behavior of the Portevin-Le Chatelier effect in an AlMg alloy containing precipitates," *Mater. Sci. Eng. A*, vol. 639, pp. 37–41, 2015.

[74] C. Bernard, J. Coër, H. Laurent, P. Y. Manach, M. Oliveira, and L. F. Menezes, "Influence of Portevin-Le Chatelier Effect on Shear Strain Path Reversal in an Al-Mg Alloy at Room and High Temperatures," *Exp. Mech.*, vol. 57, no. 3, pp. 405–415, 2017.

[75] M. A. Iadicola, T. Foecke, and S. W. Banovic, "Experimental observations of evolving yield loci in biaxially strained AA5754-O," *Int. J. Plast.*, vol. 24, no. 11, pp. 2084–2101, 2008.

[76] J. B. Le Cam, E. Robin, L. Leotoing, and D. Guines, "Calorific Signature of PLC Bands Under Biaxial Loading Conditions in Al-Mg Alloys," *Conf. Proc. Soc. Exp. Mech. Ser.*, vol. 8, no. January, pp. 31–38, 2014.

[77] D. G. E. Robin and J. Le Cam, "Effects of Strain Path Changes on the Kinematics and the Intrinsic Dissipation Accompanying PLC Bands in Al-Mg Alloys," *Exp. Mech.*, vol. 59, no. 7, pp. 963–977, 2019.

[78] ASTM, "ASTM E112-13: Standard test methods for determining average grain size," 2013.

[79] Y. Seymen, B. Güler, and M. Efe, "Large Strain and Small-Scale Biaxial Testing of Sheet Metals," *Exp. Mech.*, vol. 56, no. 9, pp. 1519–1530, 2016.

[80] J. Blaber, B. Adair, and A. Antoniou, "Ncorr : Open-Source 2D Digital Image Correlation Matlab Software," *Exp. Mech.*, vol. 55, no. 5, pp. 1105–1122, 2015.

[81] B. Güler and M. Efe, "Forming and fracture limits of sheet metals deforming without a local neck," *J. Mater. Process. Technol.*, vol. 252, no. February 2017, pp. 477–484, 2018.

[82] J. Kang *et al.*, "Shear localization and damage in AA5754 aluminum alloy sheets," *J. Mater. Eng. Perform.*, vol. 17, no. 3, pp. 395–401, 2008.

[83] S. Yoshida and S. Toyooka, "Field theoretical interpretation on dynamics of plastic deformation-Portevin-Le Chatelie effect and propagation of shear

band," *J. Phys. Condens. Matter*, vol. 13, no. 31, pp. 6741–6757, 2001.